Dynamics and control of large-scale fluidized bed plants for renewable heat and power generation

Applied Thermal Engineering 219 (2023) 119591

Contents lists available at ScienceDirect

Applied Thermal Engineering

journal homepage: www.elsevier.com/locate/apthermeng

Research Paper

Dynamics and control of large-scale fluidized bed plants for renewable heat and power generation

Guillermo Martinez Castilla [a,*], Rubén M. Montañés [b], David Pallarès [a], Filip Johnsson [a]

[a] Chalmers University of Technology, Division of Energy Technology, Hörsalsvägen 7B, Gothenburg 412 96, Sweden
[b] SINTEF Energy Research, Sem Saelandsvei 11, Trondheim NO-7465, Norway

ARTICLE INFO

Keywords:
Plant flexibility
Dynamic modeling
Simulation
Thermal power plant
Fluidized bed combustion
District heating

ABSTRACT

As the share of variable renewable electricity increases, thermal power plants will have to adapt their operational protocols in order to remain economically competitive while also providing grid-balancing services required to deal with the inherent fluctuations of variable renewable electricity. This work presents a dynamic model of fluidized bed combustion plants for combined heat and power production. The novelty of the work lays in that (i) it provides an analysis of the transient performance of biomass-based fluidized bed combustion plants for combined heat and power production, (ii) the dynamic model includes a description of both the gas and water-steam sides and (iii) the model is validated against operational data acquired from a commercial-scale plant. The validated model is here applied to analyze the inherent dynamics of the investigated plant and to evaluate the performance of the plant when operated under different control and operational strategies, using a relative gain analysis and a variable ramping rate test.

The results of the simulations reveal that the inherent dynamics of the process have stabilization times in the range of 5–25 min for all the step changes investigated, with variables connected to district heating production being the slowest. In contrast, variables connected to the live steam are the fastest, with stabilization times of magnitude similar to those of the in-furnace variables (i.e., around 10 min). Thus, it is concluded that the proper description of the dynamics in fluidized bed combustion plants for combined heat and power production requires modeling of both the gas and water sides (which is rare in previous literature). Regarding the assessment of control strategies, the boiler-following and hybrid control (combined fixed live steam and sliding pressure) strategies are found to be able to provide load changes as fast as −5%-unit/s, albeit while causing operational issues such as large pressure overshoots. The relative gain analysis outcomes show that these control structures do not have a steady-state gain on the power produced, and therefore it is the dynamic effect of the steam throttling that triggers the rapid power response. This study also includes the assessment of a turbine bypass strategy, the results of which show that it enables fast load-changing capabilities at constant combustion load, as well as decoupling power and heat production at the expense of thermodynamic losses.

1. Introduction

Variable renewable electricity (VRE) sources are predicted to increase their share in the worldwide electricity generation from 25 % in 2016 to 33 % in 2025 and by 2050 they are expected to play a crucial role in the electricity production capacities of most European countries [1,2]. Such a rapid evolution of non-dispatchable electricity generation is expected to pose serious challenges to the power grid stability owing to the inherent variability of VRE sources. In addition, the value of VRE will decrease when increasing its share unless flexibility in the demand (including storage) is employed, i.e., through the application of variation management strategies [3]. In most current energy systems, thermal power plants compensate for the fluctuating power generation from VRE sources, providing flexibility. Therefore, it is expected that with increasing shares of VRE, thermal power plants will have to meet higher flexibility requirements [4], i.e., ensuring faster load changes, increasing their load range and/or increasing their product portfolio [5]. At the same time, these plants will need to be climate-neutral. Biomass-fired thermal power plants could contribute to a power system with net-zero greenhouse gas emissions – or even negative emissions, if applied together with carbon capture and storage (CCS) [6] and the use of sustainable biomass sources. In the Nordic countries, thermal power plants, with the exception of nuclear installations, operate as combined heat

* Corresponding author.
E-mail address: castilla@chalmers.se (G. Martinez Castilla).

https://doi.org/10.1016/j.applthermaleng.2022.119591
Received 4 February 2022; Received in revised form 19 October 2022; Accepted 27 October 2022
Available online 1 November 2022

Nomenclature

Greek

α	heat transfer coefficient
β	Baumann factor
η	efficiency
θ	valve oppening
λ	relative gain coefficient, thermal conductivity
ρ	density
τ	stabilization time, time constant
ψ	enhancement factor

Latin

A	area
AP	absolute percentage error
Bo	boiling number
C	controller, pre-exponential factor, valve flow coefficient
c	heat capacity
Co	Convection number
d	diameter
dp	pressure drop
E	total energy
F	flow rate
G	static gain matrix, transfer function, mass flow density
h	specific enthalpy
HV	heating value
I	instrument
K	flow area coefficient, friction loss coefficient, gain
L	level
LF	length factor
m	mass flow through a pipe, total mass
n	number
Nu	Nusselt number
P	power, pressure
Pr	Prandtl number
p	pressure
Q	heat flow
R	resistance
s	thickness
T	temperature
t	time
x	variable, steam quality
y	variable

Subscripts

a	arrangement
c	controller, condensate
comb	combustion
crit	critical point
el	electrical
f	fuel, friction
fw	feed water
g	gas
hyd	hydraulic
is	isentropic
L	liquid
L,M	logarithmic mean
m	matrix element, measured
mech	mechanical
n	element
nom	nominal
o-c	for other control loops closed
o-o	for other control loops open
p	constant pressure
s	simulated, steam
t	turbine
tp	two-phase
v	vapor, valve
vap	vaporization
w	wall
0	initial, reference
∞	final

Abbreviations

BF	boiler following
BFB	bubbling fluidized bed
CCS	carbon capture and storage
CFB	circulating fluidized bed
CHP	combined heat and power
CP	centrifugal pump
CV	controlled variable
DH	district heating
DMC	dynamic matrix control
DRGA	dynamic relative gain analysis
ECO	economizer
HPT	high pressure turbine
FB	fluidized bed
FBC	fluidized bed combustion
FF	feed-forward
FG	flue gas
FP	floating pressure
FWH	feed water heater
ICPD	integrated control plant design
IPT	intermediate pressure turbine
LPT	low pressure turbine
MPC	model predictive control
MV	manipulated variable
OFWH	open feed water heater
PI	proportional integral
RGA	relative gain analysis
SP	set-point
SH	superheater
TF	turbine following
VRE	variable renewable electricity
VRR	variable ramping rate

and power (CHP) plants, i.e. producing hot water for district heating (DH) or steam for industrial facilities, as well as generating electricity. Typically, due to the heating demand in biomass-rich regions, the production of DH is the main economic incentive for these plants. Consequently, the production level has traditionally been planned to cover the aggregated DH demand in conjunction with other heat-only boilers or CHP plants in the local DH system [7]. With an increased share of VRE, given its low operating costs, it seems likely that CHP plants will need to be more flexible in order to maintain competitiveness, providing faster and larger load changes and increasing their operational and product flexibility levels. As identified in a previous publication [8], current research towards improving the flexibility of biomass-based CHP plants mainly involves: (i) the implementation of energy storages within the plant [9,10]; (ii) the investigation of primary frequency response capabilities [11,12]; (iii) the decoupling of power and heat production [13]; (iv) increasing the fuel flexibility [14]; and (v) retrofitting the furnace for the coproduction of biogas [15].

Control solutions for current thermal power plants [16] are often based on traditional industrial practices and are not optimized for flexibility. Moreover, process optimization of CHP plants has not placed an

emphasis on how flexibility requirements influence the operation and profitability of the plant. Thus, with new requirements regarding flexibility, there is a need to understand the possibilities and limitations for transient operation of CHP plants. Different supervisory control strategies (here defined as the control layer responsible for regulating the production of heat and power in the hour-minute timeframe [17,18]) for thermal plants have been proposed and investigated through process simulations, as reported in the literature [19,20]. However, the optimization strategy for biomass-based CHP plants presents two new challenges: the specific combustion behavior of fluidized beds (with slower response time coupled to the larger fuel particles used and the thermal inertia of the bed material) and the fact of having two products (heat and power) in the business planning. While the first aspect is given by the technology choice, the second includes the strategic perspective on the product and customers portfolio (heat-driven or power-driven operation, maximized revenue operation). It is known that the chosen strategy has an impact on plant efficiency, as well as on the ability to provide fast load changes while maintaining process safety. A crucial question is whether the live steam pressure should be fixed (such as in turbine-following and boiler-following modes) or not fixed (sliding pressure, floating pressure and hybrid control modes). Although these strategies have been published and implemented in industry for some decades, different nomenclatures, classification systems and definitions are given for these strategies in the literature. Furthermore, as biomass-fired plants are expected to expand their product portfolio, allowing the decoupling of heat and power production and possibly also incorporating the co-production of biofuels, new control strategies will be required.

Besides control, operational strategies such as steam extractions and turbine bypass are commonly applied to increase the flexibility of thermal power plants [21,22], especially when they are deployed with a thermal energy storage in the form of steam accumulation [10]. Other alternatives to secure flexibility are also available, such as making the extracted steam to instead be condensed with the DH water, which can buffer the variations caused by the steam extraction.

Dynamic power plant modeling and simulation can be used to evaluate the transient capabilities of existing and future thermal power plants. An extensive up-to-date review of thermal power plant dynamic simulations has been published by Alobaid et al. [23], in which they highlight the lack of modeling studies of biomass-fired CHP plants that take into account the dynamics of the combustion chamber. Avaginos et al. [24] have recently presented a dedicated review of the process modeling of solid-fuel plants, in which once again the lack of publications focusing on biomass-fired CHP units was noted. Literature on the dynamics of CHP plants is scarce (the above-referred [10,12], together with [25]) and focuses on the water-steam side of coal or waste-fired units. In this regard, it is important to point out the fact that the dynamics of a given combustion plant are characterized by the combustion technology used, and therefore, the literature survey presented below reviews studies focusing on the dynamics of FBC plants (for which a vast majority are coal-fired power plants, but CHP biomass-fired plants are common in bioenergy-intensive regions).

Due to their strong mixing and heat transfer capabilities, fluidized bed combustors (FBCs) are the preferred option for burning low-grade solid fuels (such as biomass) at large scales [26]. As a consequence, FBCs represent a substantial percentage of the solid-fuel furnaces in regions with strong availability of biomass and well-established CHP plants [27,28]. A common feature of the FBC technology is the large amount of solids inventory in the furnace, which yields a high thermal inertia, strong intercoupling among process parameters and non-linear transients [29,30,31] all of which are crucial aspects to be addressed when attempting to increase the flexibility characteristics of FBC plants.

When it comes to evaluating the flexibilization of FBC plants, Hultgren et al. [32] employed a process model of a coal-fired CFB boiler developed in APROS to perform a control design analysis using static and dynamic relative gain analyses (RGA and DRGA, respectively), in which they identified substantial control loop interactions, i.e., the manipulation of one input affected several outputs. Their work was subsequently expanded [33], whereby a simple mass storage capacity model was developed to carry out an integrated control process design (ICPD) and optimize the dynamic performance of the steam side of a coal-fired CFB unit. The results showed that an ICPD with boiler-following control was capable of providing efficient load tracking, although the authors concluded that more detailed mechanistic modeling would be required to derive more comprehensive results. Beiron et al. [8] developed and validated a dynamic process model in Modelica and used it to investigate the transient characteristics of a waste-fired FBC-CHP steam cycle. Even though the model did not include a representation of the gas side dynamics, the results of that study showed that the process reacted more slowly to changes in the boiler load than to changes in the DH system. Similarly focusing on the dynamics of waste-fired plants, Zimmerman et al. [34] compared different control strategies, concluding that feed-forward (FF) model predictive control (MPC) is the best system for disturbance rejection, i.e., to deal with unplanned changes. Gao et al. [30] have presented a dynamic 1D furnace model combined with a boiler model (including the drum and the tubes), and validated it against a 300-MW condensing unit. The overall model was thereafter used to investigate control strategies for quick load changes based on the fuel accumulation within the furnace, such that it achieved a load ramping rate of 1.7–2.5 %/min. The model in [30] was linearized and used for MPC by Zhang et al. [35], who successfully tested a dynamic matrix control (DMC) strategy for different ramping rates. Kim et al. [36] developed a dynamic model that accounted for both the in-furnace (1.5D, detailed in [37]) and water-steam sides, which after validation with steady-state data from a 500-MW unit, was used to quantify the transient response of the steam temperature following changes in the feedwater and fuel flows. Stefanitsis et al. [38] presented a 1D dynamic model of CFB furnaces that was built in APROS and validated with data from a 1-MW pilot unit and which was thereafter used to investigate the transient performance of the cited plant after a thermal energy storage unit in the form of hot bulk solids was implemented within the plant; they concluded that the stabilization time for load changes was reduced when adding storage (and thereby decreasing the solids inventory within the furnace). Most of the literature cited above has focused on CFB units. However, with respect to BFB plants, it is worth mentioning the work of Zlatkovij et al. [39], in which a linearized dynamic model of a biomass-fired BFB boiler that included a 0-dimensional description of the gas side was used to test and compare MPC strategies for disturbance rejection, concluding that FF-MPC was the preferred option (as in [34]).

In summary, regarding the literature on flexibility studies, studies of FBC units have mostly been concerned with coal-fired condensing plants, while those focused on CHP plants have mostly investigated gas-fired units [40,41]. Thus, there is a scarcity of publications regarding the flexibility of FBC-CHP plants with biomass as the fuel, the importance of which has recently been reviewed by Atsonios et al. [42]. Note that the general differences between biomass-fired plants and coal-fired ones are expected to yield fundamentally different plant dynamics (since biomass plants are smaller, operating in CHP mode, biomass has a higher volatile and hydrogen content than coal). Furthermore, works involving FBC units generally lack a model of the gas side capable of describing the dynamics of the combustion process in parallel with the dynamics of the Rankine cycle. This hinders examination of the impacts on process dynamics of variables that are crucial for FBC operation such as the circulation and inventory of solids, emissions, or fuel reactivity. The authors of the present work have recently presented a validated mechanistic dynamic model for the in-furnace side of industrial-sized FBC furnaces [29], which was used to investigate the dynamics of CFB and BFB combustion processes. The model was used to elucidate the stabilization times of the temperature and heat extraction in different regions of the furnaces. In [31], the in-furnace model was used to study the sensitivity of the computed in-furnace stabilization times to mechanisms such as fluid dynamics, heat transfer and fuel combustion. However, the

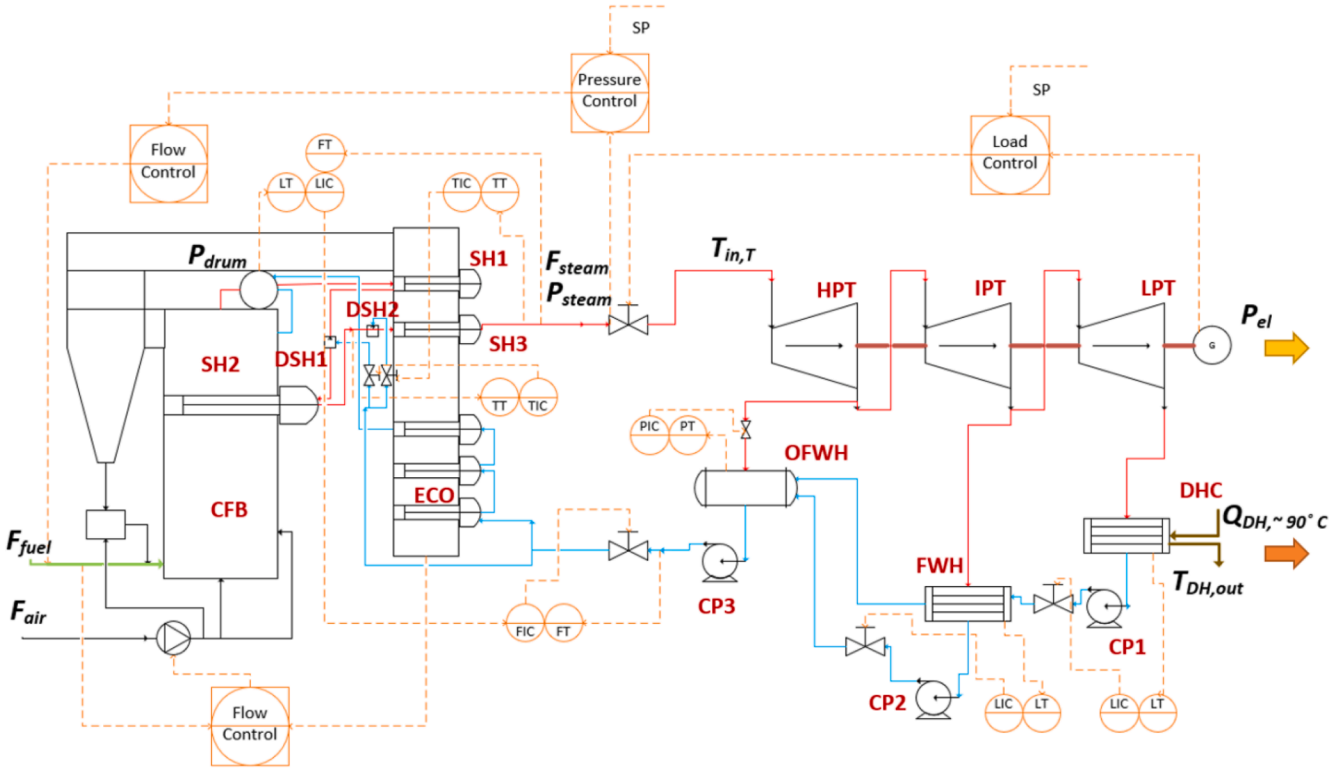

Fig. 1. Schematic process diagram of the reference plant. Steam and water lines are represented by red and blue lines, respectively. Regulatory and supervisory control structures of the reference plant are included in orange, with signals represented in dashed lines. F: mass flow. T: Temperature. Q: heat load. P: electrical power and pressure. SP: Set point. SH: Superheater. DSH: desuperheater. ECO: economizer HPT: high pressure turbine. IPT: intermediate pressure turbine. LPT: low pressure turbine. DHC: District heating condenser. FWH: feedwater heater. CP: centrifugal pump. (For interpretation of the references to colour in this figure legend, the reader is referred to the web version of this article.)

investigations in [29,31] focus on the in-furnace side and model studies considering the interplay between this and the water/steam side remain as a main gap in literature.

The aim of this work is to evaluate the transient operation of biomass-based FBC-CHP plants in terms of the potential to operate in a future electricity system in which volatile wholesale prices for electricity can be expected such that flexibility of plant operation will be valued higher than it is at present. To identify the limits of flexibilization, the present study focuses on operational and control strategies that can maximize the plant ramp rate and extend the operational boundaries in the hour-minute timeframe, i.e., expand the product output area. This paper includes a comprehensive description of the main supervisory control strategies for load changes that can be applied to FBC-CHP plants. The in-furnace side model presented and validated previously in [29,31] is here connected to a model of the water-steam side. The resulting merged model is validated here with industrial plant data, and then used to: (i) perform a relative gain analysis (RGA), to evaluate the interactions between the inputs and outputs of the plant so as to assess the controllability of the process; (ii) characterize the inherent (uncontrolled) dynamic behavior of the plant; and (iii) test how different control and operational strategies could provide fast load changes.

The novelty of the work lays in that (i) it analyses the transient performance of biomass-based FBC-CHP plants, (ii) the dynamic model includes a description of both the gas and water-steam sides, and (iii) the model is validated against operational data acquired from a commercial-scale plant.

2. The reference plant

The present work uses a 100-MW_{th} biomass-fired CFB boiler located in Karlstad (Sweden) as the reference plant, as it has a size and plant layout that is representative of biomass-fired FBC-CHP plants (typically ranging from 30 to 400 MW_{th}, see for instance [43]). The unit has also been used for the calibration and validation of the in-furnace side model [29]. The unit is normally operated with wood chips with moisture content of 50 %–55 % (for detailed fuel composition, see [29]). A simplified process diagram with the main process variables and components is shown in Fig. 1. The plant consists of the CFB furnace, a convective flue gas path, comprising three economizer tube bundles (ECO), two superheaters (SH1 and SH3), and a three-section air preheater (not included in Fig. 1), an in-furnace superheater (SH2), a steam drum, a steam turbine with two intermediate extractions (each turbine section named HPT, IPT and LPT), a steam condenser (DHC) in which DH water at ~90 °C (the main product of the plant) is produced, and one closed and one open feedwater heater (FWH and OFWH, respectively). Table 1 lists the main design data for the reference plant operated at full load.

Table 1
Design data of the reference plant.

Boiler capacity	100	MWth
Live steam mass flow	28.9	kg/s
Live steam pressure	67	bar
Live steam temperature	505	°C
Electrical power	20.2	MW
District heating load (DHC)	56.8	MW
Power-to-heat ratio	0.36	–
Drum pressure	74.3	bar
Steam turbine exhaust pressure	1.2	bar
Feedwater temperature	270	°C

2.1. Flue gas side

The fuel is combusted primarily in the CFB furnace, where the solids carried by the gas up to the furnace top and exit ducts are separated from

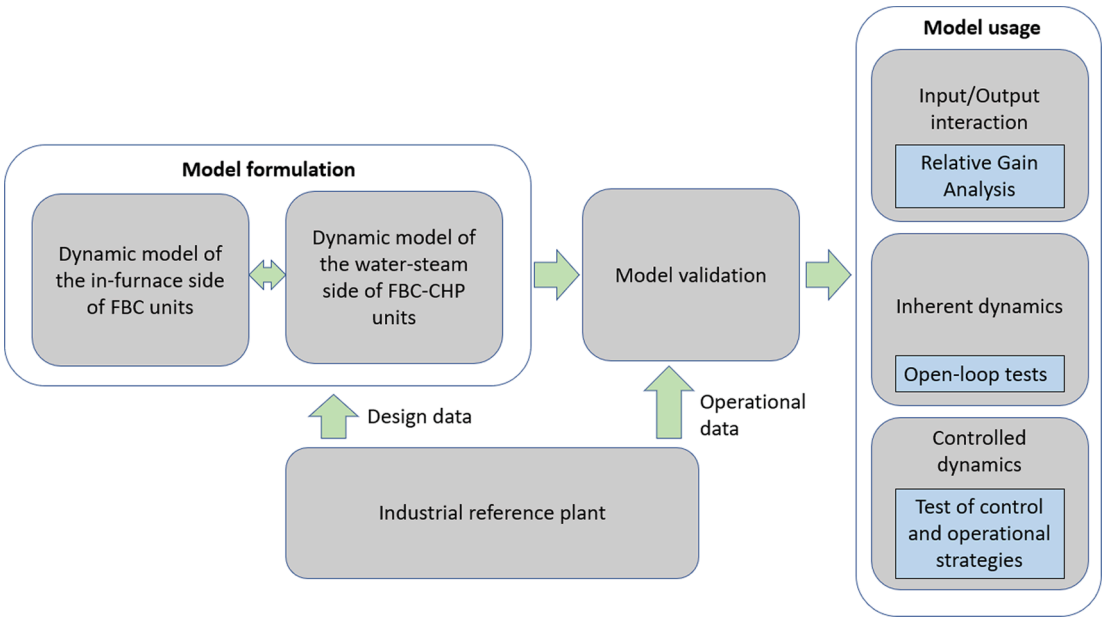

Fig. 2. Summary of the methodology followed in the present work.

the gas in two parallel cyclones and returned to the furnace via the return legs, where the fresh fuel is fed. The furnace has a height of 20 m. Air is fed into the furnace partly as primary air, which fluidizes the bottom bed, and partly as secondary air at a height of 5 m. The immersed superheater tube bundle SH2 is located at a height of 11 m. Most of the furnace walls consist of membrane walls that evaporate the feedwater. The hot flue gases leaving the cyclones flow through the convection path, where the superheaters, economizers and air preheaters are transversally located, before progressing towards the gas cleaning system and flue gas condenser (not included in Fig. 1).

2.2. Water-steam side

The water-steam cycle is a conventional subcritical, single-pressure system that is typical of CHP plants in Sweden. The subcooled feedwater is first preheated in the economizer ECO before being fed into the drum, from which the water is naturally circulated through the evaporator, i.e., the downcomer and riser tubes located in the furnace walls. The evaporating mixture is separated in the drum prior to the steam superheating. Desuperheaters (DSHs) spraying subcooled feedwater are located between the superheating stages for temperature control. The live steam is thereafter expanded in the steam turbine, producing electricity and DH water. As part of the heat integration of the plant and bearing in mind that DH water is the main product in the business and production planning, the DH water that flows through the turbine condenser DHC has previously been preheated up to 70℃ in the flue gas condenser (not included in Fig. 1). Intermediate-pressure steam at 6 bar and 4 bar (at full load) are extracted for the OFWH and FWH, respectively, with the former being used as a deaerator to remove oxygen and other non-condensable species. The feedwater pump CP3 recirculates the water from the deaerator back to the boiler.

2.3. Control

Conventional power plant regulatory control loops [44] in the water-steam side to maintain the stability and controllability of the plant, as shown in Fig. 1. The levels of the DHC and FWH are controlled by manipulating the condensate pump control valves. For inventory consistency, the OFWH level is not controlled continuously but is maintained within certain safety limits by the addition/removal of make-up water to/from the loop (not included in Fig. 1). The pressure of the OFWH is controlled by manipulating the control valve placed in the steam extraction. The feedwater pump and control valve located downstream of the OFWH are used to control the level of the drum through a three-point control system. Regarding the supervisory control layer, a conventional boiler-following strategy (see Section 3.2.2 for more details) is implemented, as shown in Fig. 1. Note that due to the absence of a condenser operating with cooling water, the output of the plant follows a constant power-to-heat ratio. The controller of the air mass flow is connected to the fuel flow controller using an FF signal from the oxygen concentration exiting the furnace. The air primary/secondary split depends on the fuel flow, i.e., boiler load. Finally, the mass flow of feedwater sprayed in the DSHs is used to control the steam temperature after each superheater section.

3. Methods

Fig. 2 presents the overall methodology employed in this work. First, a mechanistic dynamic model of an FBC-CHP plant is built, which is presented in Section 4. The model is calibrated and validated (Section 4.4) using steady-state and transient operation data from an industrial unit. Model simulations are then used to carry out the following three analyses:

(1) Steady-state interactions between the main inputs and outputs of the plant are investigated through an RGA (Section 5.1), which is used to assess the steady-state performance of the control structures presented in Section 3.1.
(2) The inherent dynamics of the process are explored through simulations of open-loop tests (Section 5.2.1).
(3) The control structures and operational strategies presented in Section 3 are tested dynamically, so as to study the capabilities of the controlled process to provide fast load changes in different future energy markets (Sections 5.2.2 and 5.2.3).

3.1. Control structures for load changes in CHP plants

As stated in a previous publication [16], boiler control involves the regulation of the outlet conditions of steam flow, temperature, and pressure to attain their desired values. Supervisory control structures of boiler-turbine units are in charge of controlling the plant outputs in a

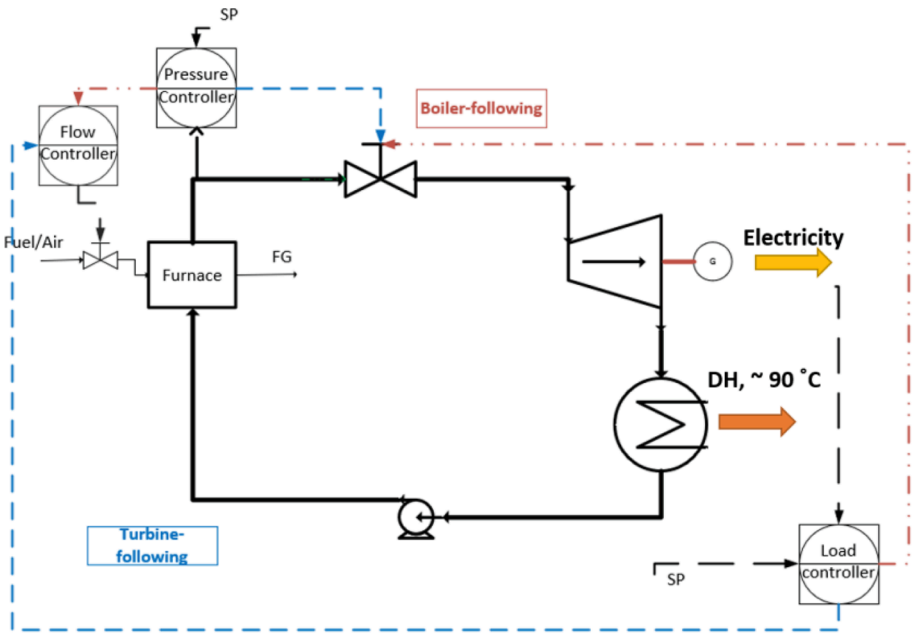

Fig. 3. Fixed pressure operation strategies for load changes. Blue lines represent the turbine-following strategy, while the red lines indicate the boiler-following strategy. SP, Set-point; FG, flue gas. (For interpretation of the references to colour in this figure legend, the reader is referred to the web version of this article.)

minute-hour timescale, and they handle disturbances connected to fuel heating value variations and load changes. Two main control strategies exist: one based on fixed live steam pressure, and the other one allowing the live steam pressure to change with load (in a controlled or uncontrolled manner). Jonshagen and Genrup [19] performed a thermodynamic assessment of the steady-state implications of fixing or not fixing the steam pressure in CHP units and concluded, similar to the findings of others [45], that a hybrid strategy is the most beneficial approach from the perspective of efficiency. Within each of these strategies, several control structures can be used, and the studies in the literature are often discrepant in terms of the terminology and classification of these structures, which are applied to industrial facilities but lack application to CHP plants. This section describes the control structures for load changes that are investigated and tested in this work (see Section 5.2). The work of Zotică et al. [20] describes an up-to-date plantwide control structure design methodology applied to heat-to-power cycles, to which the reader is referred for a complete description of the general methodology followed when designing some of the control structures described herein.

3.1.1. *Fixed pressure operation*

Turbine following: In this operation mode (indicated by blue lines in Fig. 3) the turbine follows the response of the boiler. Thus, the master controller uses the combustion load (fuel/air flows) to control the power plant outputs, and the steam valve is used to keep the steam pressure at the desired set-point. When, for instance, increasing the combustion load, the steam pressure will increase and, in order to keep a constant live steam pressure, the steam control valve will gradually open. The major drawback of this strategy is that it is characterized by a large time constant connected to the combustion load and, therefore, it is not

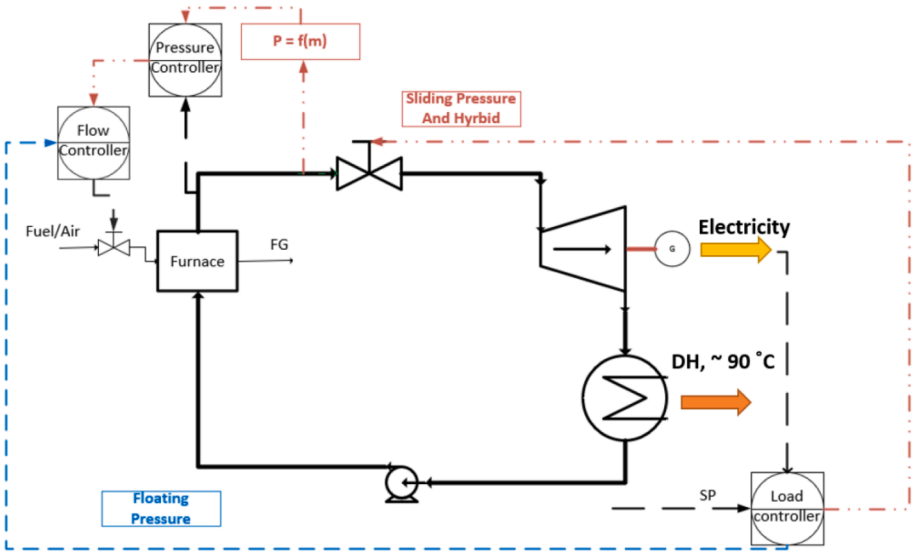

Fig. 4. Variable pressure control strategies for load changes. Blue lines represent the floating pressure strategy, while the red lines indicate the sliding pressure and hybrid control modes. SP, Set-point; FG, flue gas. (For interpretation of the references to colour in this figure legend, the reader is referred to the web version of this article.)

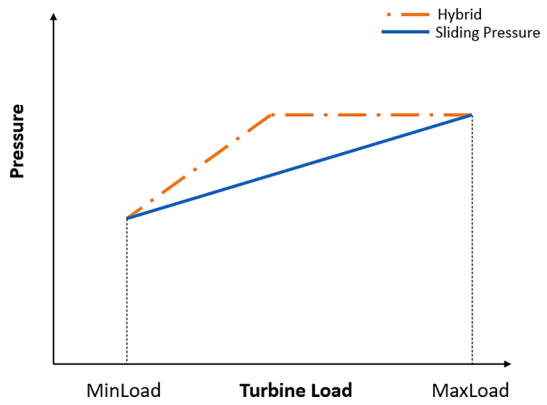

Fig. 5. Variable pressure curves for the pure sliding pressure [46] and hybrid control [47,48] modes.

suitable for fast load changes.

Boiler following: The rationale for boiler-following control (red lines in Fig. 3) is the opposite to that for turbine-following control: the master load controller now manipulates the live steam control valve and the combustion load is used to control the steam pressure. Following a load change, the boiler utilizes the energy stored in the drum to provide a faster response than that seen with turbine-following, although the pressure control is less stable and efficient [16].

3.1.2. Variable pressure operation

Floating pressure: In this mode (blue lines in Fig. 4), the live steam pressure is not controlled but instead results from the energy balance in the boiler as the master controller manipulates the combustion load. The main advantages of this strategy are the reduction in the amount of power required by the feedwater pump at partial loads and the avoidance of live steam throttling. However, not controlling the pressure may introduce issues related to steam pressure gradients in the turbine blades. In addition, the mean temperature of the heat supply is reduced at partial loads because evaporation occurs at lower temperatures, which has a negative effect on the total efficiency of the plant [19].

Sliding pressure: This mode (illustrated by red lines in Fig. 4) was first suggested by Klefenz [46] as a way to solve some of the operational problems that arise at floating pressure mode for coal-fired power plants (i.e., plants of larger size than the biomass-fired plant analyzed here). In this control structure, the pressure is controlled but not fixed; instead, its set-point follows a pre-defined curve that varies with turbine load. Under this mode, it is common to use the mass flow as a measurement of the power [20,46] (see Fig. 4).

Hybrid control: Sliding pressure control can be purely sliding or hybrid in form, depending on the pressure curve applied. Fig. 5 shows a pressure curve that combines the use of sliding pressure control at lower loads and the boiler-following strategy at higher loads. Hybrid control operation was developed as a strategy to avoid the issues connected with fixed pressure operation (i.e., losses related to live steam throttling) and with floating operation (i.e., slow response), and it has been studied over the past decades [47,48] in coal-fired plants. For simplicity, only the hybrid type of sliding control is included in the present study, with the switch between constant and variable pressure being set to occur at 75 % load. A detailed optimization study based on active constraint regions [49] would be needed to determine the optimum switching point. Note that the pressure curves shown in Fig. 5 differ from those typically found in combined cycle power plants, where the slow response of the steam cycle is not a problem due to the rapid dynamics of the gas turbine, which yields variable pressure operation of the steam turbine at higher loads and constant pressure operation at lower loads.

A summary of the relationships between manipulated variables (MVs) and controlled variables (CVs) of each strategy is shown in Table 2, while the implementation of each strategy in the model is provided in Section 4.2 (all tuned parameters of the controllers are listed in Table 9).

Table 2
CV-MV relationship of the control strategies included in this work.

Control structure	Controlled variable (CV)		Manipulated variable (MV)
Turbine following	Generated power/DH	↔	Combustion load
	Live steam pressure	↔	Live steam valve
Boiler following	Generated power/DH	↔	Live steam valve
	Live steam pressure	↔	Combustion load
Floating pressure	Generated power/DH	↔	Combustion load
Sliding pressure/ Hybrid control	Generated power/DH	↔	Live steam valve
	Live steam pressure (controlled but not fixed)	↔	Combustion load

Table 3
Controlled and manipulated variables defined for the relative gain analysis.

CVs	MVs
Live steam temperature, T_{steam}	Combustion load, Q_{comb}
Live steam pressure, P_{steam}	Live steam valve opening, $Valve_{steam}$
Power produced, P_{el}	DSH spray water flow, F_{DSH}

3.2. Relative gain analysis

RGA is a well-established methodology [50] for evaluating the controllability of a process with multiple inputs and outputs such as an FBC-CHP plant, e.g., a CFB combustor [32]. In a system with m manipulated variables (MVs) and n controlled variables (CVs), the RGA is based on calculating the static gain matrix G through Eq. (1), computing the relative gain coefficients λ of a certain variable pairing. These coefficients are a measure of the open-loop gain of a pairing when all control loops are open ($g_{O\text{-}O}$) compared to the gain when all other control loops are closed ($g_{O\text{-}C}$) [see Eq. (2)]. The results of such a comparison are commonly used to select variable pairings that minimize the interactions with/from other loops. Thus, the optimal value of λ for a good control pairing is 1, while small positive values indicate poor controllability, values much greater than 1 identify variable pairs that would require very high controller gains, which are typically to be avoided, and negative values yield instabilities due to the sign change in the gain. Lastly, it must be mentioned that RGA requires a square system, i.e., $m = n$, although alternatives are available for non-square systems The control structure (i.e., combination of pairings) with largest amount of good pairings (close to 1) in the RGA matrix is considered the one that minimizes the degree of loop interactions.

$$RGA = G \times G^{-1} = \begin{bmatrix} \lambda_{11} & \cdots & \lambda_{1n} \\ \cdots & \cdots & \cdots \\ \lambda_{m1} & \cdots & \lambda_{mn} \end{bmatrix} \tag{1}$$

$$\lambda_{mn} = \frac{g_{O-o}}{g_{O-C}} \tag{2}$$

The CVs and MVs in the current setup of the chosen reference plant (Fig. 1) are listed in Table 3. The electrical power produced by the steam turbine is strictly linked to the load of DH produced, since there is no turbine bypass. Therefore, the plant is assumed to operate at a constant power-to-heat ratio. Thus, the three CVs available for control are the live steam temperature and pressure and the power output. Note that the live steam temperature can be controlled between each of the superheater stages, and each of these would represent an independent CV, although only one has been taken into account for the sake of simplicity. Having three CVs, the three MVs chosen are the combustion load, live steam valve, and DSH spray water flow. The combustion load can be split into several MVs, although it is here assumed that the fuel and air flows are always manipulated together, i.e., changed simultaneously. To compute

Table 4
Disturbances and their magnitudes thereof simulated in the open-loop tests.

Input variable step-changed	Step-change magnitude
Combustion load, Q_{comb}	±20 %
Fuel heating value, HV_f	±20 %
DH water flow, F_{DH}	±20 %
DH water inlet temperature, $T_{DH,in}$	±20 %

Table 5
Process variables tracked during the open-loop tests.

Main process variable, *abbreviation*, [unit]
Power produced, P_{el}, [MW]
DH load, Q_{DH}, [MW]
DH water outlet temperature, $T_{DH,out}$ [°C]
Live steam mass flow, F_{steam} [kg/s]
Live steam pressure, P_{steam} [bar]
In-furnace total heat to the waterwalls, Q_{wall} [MW]

Table 6
Definition of scenarios and cases included in the variable ramping rate analysis.

Scenario	Description
I	100 % to 50 % load change
II	50 % to 40 % load change

the matrix G, changes in the MVs of −10 % were simulated when the plant was running at 100 % load. The gain of the three CVs was then computed from the variable responses after stabilization. Since the present study focuses on the supervisory control layer, the regulatory control loops are excluded from the analysis, i.e., they are assumed to remain the same as in the current plant setup.

3.3. Dynamic analysis

3.3.1. Inherent process dynamics – Open-loop tests

Open-loop tests are simulated to obtain the inherent transient performance of the process after a certain disturbance/input change occurs in the absence of supervisory control loops, i.e., only the regulatory control loops are activated. Individual step changes in the set-points of the main process inputs and disturbances are introduced in the model. To ensure that the system is perturbed sufficiently to distinguish deviations between test cases, the step-change magnitude is ±20 % and is introduced when the process is running steadily at 80 % load. To evaluate the effect of the boiler load on the inherent process dynamics, the analysis is also conducted when the process runs at 70 % load. Note that, as pointed out in [20], the steam pressure is often considered to be supervisory control and, therefore, it is not controlled here. The inputs that are changed are listed in Table 4, while the variables used to characterize the dynamic performance of the process are listed in Table 5. In this work, the open-loop performance of the process is assessed in terms of the total stabilization time, i.e., the time that it takes for a certain process variable to remain within an error band of ±10 % of the total change in steady-state values [Eq. (3)].

$$t_s = \tau\big|_{y_0 \to y_\infty \mp 0.1(y_0 - y_\infty)} \tag{3}$$

3.3.2. Controlled process dynamics - variable ramping rate analysis

To assess the capabilities of the controlled plant to provide load changes at different ramp speeds, a variable ramping rate analysis is performed. Two load change scenarios are considered (see Table 6): I) 100 % to 50 % and II) 50 % to 40 % load changes. Scenario I is based on studies (see, for example, [51]) that have proposed that thermal power plants will be required to provide not only faster but larger load changes when running at full load. Scenario II represents the more moderate load changes required when the plant is run at partial load (for most of its operational time). Furthermore, it is well known [52] that some operational issues arise when running at minimum loads, such as the temporary appearance of too-low steam flow in certain sections of the turbine. Four different ramping speeds are investigated in the present work for each scenario. The combinations of these results in eight cases with different load change rates (in %-unit/s) that are shown in Table 7. To quantify the responses to each control strategy for each of the simulated cases, the rise time of the generated power is computed, defined as the time that it takes for the output power to go through the 10 %–90 % response window [53].

Table 7
Relative magnitudes of each of the cases simulated in the variable ramping rate analysis.

	Very slow	Slow	Fast	Very fast
Scenario I	−0.005 %-unit/s	−0.05 %-unit/s	−0.5 %-unit/s	−5 %-unit/s
Scenario II	−0.001 %-unit/s	−0.01 %-unit/s	−0.1 %-unit/s	−1 %-unit/s

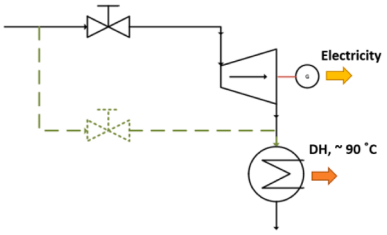

Fig. 6. Turbine bypass scheme. Note that the bypassed steam is a fraction of the live steam and can be chosen freely.

3.3.3. Turbine bypass

In order to investigate the potentials of other operational strategies to provide fast load changes, the dynamic performance of a turbine bypass is evaluated. Since the effect of steam extractions on power output is maximized for higher pressures [54], the steam bypass from the high-pressure line, i.e., prior to the steam turbine, is studied. The bypassed steam is condensed in the DHC to producing DH water (see Fig. 6). Note that a valve is added to regulate the steam pressure down to the DHC pressure.

The performance of the bypass is assessed for the following situations:

- The bypass valve is opened (as a 1-s ramp) to allow 3, 5 and 7 kg/s of steam to pass when the plant is running steadily at 50 % load; and
- The bypass valve is closed (as a 1-s ramp) when the plant is running steadily at 70 % load and has an initial bypass flow of 3, 5 and 7 kg/s.

4. Dynamic modeling

The reference plant described in Section 2 is modeled with a dynamic FBC-CHP plant model developed in Dymola [55], which uses the Modelica language [56]. The time resolution of the model is defined by variable optimized time step values in the order of 100 s. The model equations are solved using an explicit Runge-Kutta (ESDIRK) method which is especially suitable for initializing stiff non-linear flow models. The plant model is the result of integrating a dynamic model of the in-furnace side of the FB boiler previously developed and validated by the authors [29] with a dynamic process model of the water/steam side (similar as those in [8,57], i.e., built using the Modelon ThermalPowerLibrary [58]). Fig. 7 shows the input/output scheme of the integrated model. The in-furnace and the water/steam side models are connected through the following:

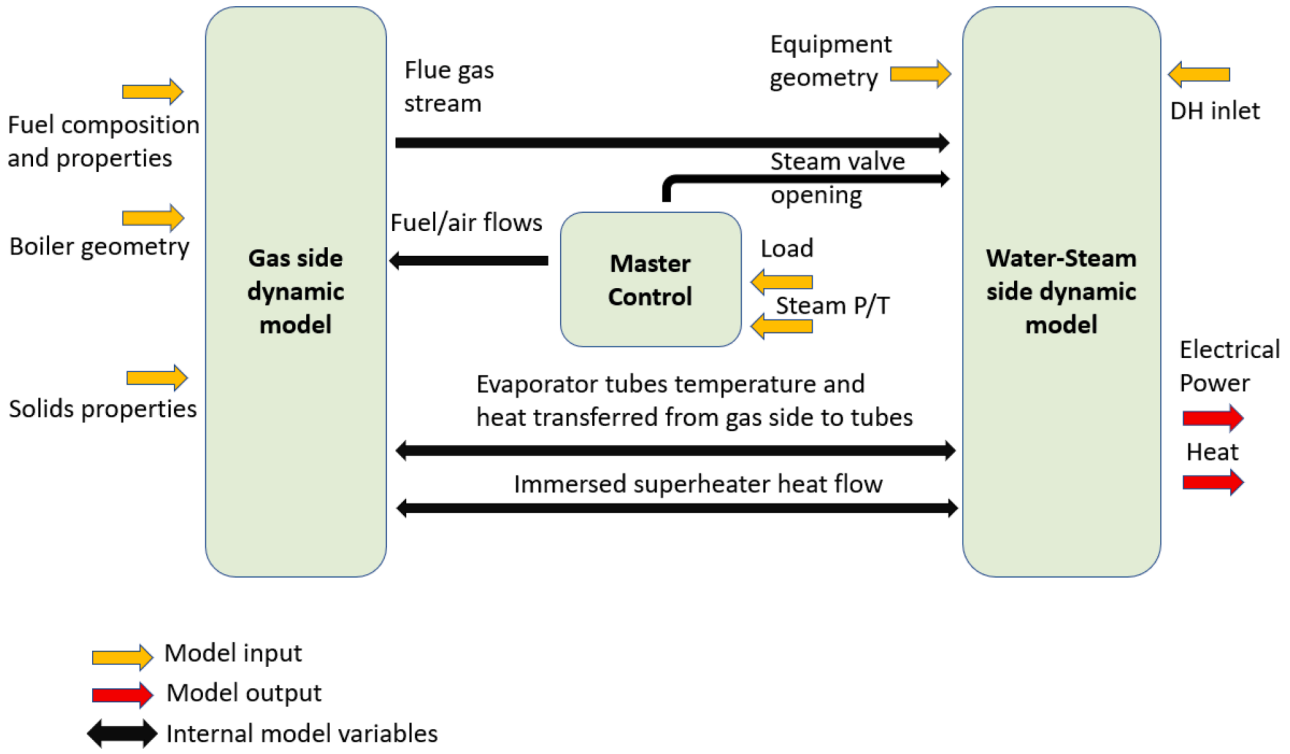

Fig. 7. Input/output scheme for the integrated dynamic model of the FBC-CHP plants.

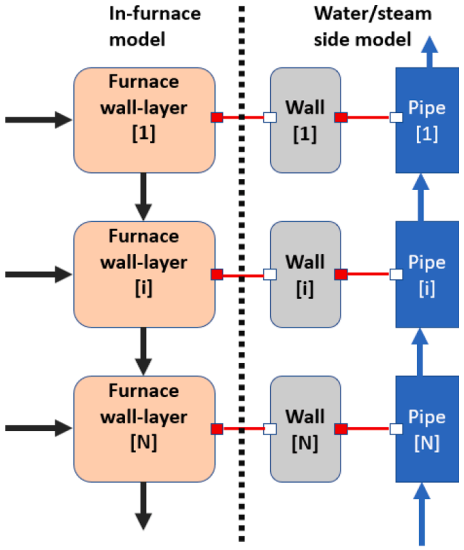

Fig. 8. Scheme of the thermal connections between the evaporator and the in-furnace solids wall layer. The vertical dashed line represents the boundary between the in-furnace and water/steam side models.

- The flue gas stream leaving the furnace enters the water/steam side model via the convection path.
- The waterwalls that make up the evaporator remove heat from the in-furnace side while evaporating the two-phase water flow, yielding a certain wall temperature. This connection, shown in Fig. 8, contains as many connections as control volumes with the waterwalls present the in-furnace side model (10 for the present case; see [29]).
- The immersed superheater located in the furnace (SH2 in Fig. 1) extracts heat from the corresponding in-furnace control volumes while superheating steam.

In the present section, the main characteristics and formulations of the model are discussed.

4.1. *In-furnace model*

The formulation, calibration and validation of the dynamic model used for the in-furnace side is presented elsewhere [29]. The in-furnace model uses semi-empirical modeling rather than pure empirical correlations, i.e., it closes mass and heat balances based on theoretical expressions containing experimental coefficients (e.g., mass transfer coefficients, velocity fields) determined from dedicated experimental campaigns. This theoretical ground gives the in-furnace model a relatively robust ground. Furthermore, the validity scope and reliability of such model for different boiler designs and conditions have recently been explored in [31]. Yet, a brief summary of the in-furnace side model is included below.

The model describes the in-furnace side of FB boilers through a number of perfectly mixed control volumes (CSTR) that exchange mass and energy. The model accounts for the three processes that govern the energy and mass transfer in FB furnaces: (i) fluid dynamics (1.5D representation, i.e., considering the wall layers hosting the internal recirculation of solids [59,60]); (ii) thermochemical conversion; and (iii) heat transfer, covering both solids convection and radiation. The model accounts for three phases: bulk solids, fuel, and gas. The fuel contains three classes to account for changes in size and density during conversion, while the gas consists of a mixture of nine components.

As shown in Fig. 7, the inputs to the in-furnace side model are the geometry of the boiler, mass flows temperature and locations of the fuel and gas streams fed, and the properties (size and density) of the bulk solids. The model solves dynamic mass and energy balances for each of the control volumes defined, solving for each of them the concentrations and mass flows of each of the phase components, as well as the temperatures and heat flows to neighboring cells and walls. To adjust the model to represent as closely as possible the reference unit, the model is calibrated by tuning the solids particle size and gas mixing using process site data.

4.2. Water/steam side model

The present section summarizes the main correlations that describe each of the water/steam side components using the lumped parameter approach, which is confirmed to be a valid assumption for dynamic power plant modeling [61]. A more extensive list of the main model equations and references is included in Appendix A (Table A1).

For all the components, geometric data (e.g., dimensions, number of tubes, tube pitch, existence of fins, metal thickness) are fed into the model according to the design of the reference plant. For those components where a 0-dimensional representation is not appropriate (e.g., a tube), a 1D discretization into a series of volumes is applied, for each of which the dynamic mass and energy balances are solved. The number of volumes in which a certain equipment can be discretized represents a compromise that is made between model accuracy and computational time in the calibration phase. The component models described below are calibrated through a pre-exponential factor in the correlations for the heat transfer coefficient, C. The model is calibrated to operational data collected at 100 % load (see Appendix A), whereas the prediction of the partial-load performance of the reference plant represents the model validation (see Section 4.4).

Regarding the gas–water/steam heat exchangers, the heat transfer on the gas side of superheaters and economizers in the convection path is modeled using a convective heat transfer coefficient for gas flowing over tube bundles [Eq. (4)], which uses the Nusselt (Nu) number correlated from VDI-Wärmeatlas [62], where λ is the thermal conductivity and d_{hyd} the hydraulic diameter of the tube. In the water/steam side model of economizers and superheaters (monophasic flow), the heat transfer is also described using a Nu-correlation as in Eq. (4), but excluding the tube arrangement factor, F_a. In the evaporator (biphasic flow) a Nu-correlation based on the Dittus-Boelter equation is used [8,63].

$$\alpha = C\frac{F_a Nu_0 \lambda}{d_{hyd}} \tag{4}$$

The pipe pressure drops in both the gas and water/steam sides are computed through a friction loss correlation based on a coefficient that assumes turbulent flow, in which K_f is the friction loss coefficient, dp_{nom} the nominal pressure drop, LF the length factor, ρ_{nom} the nominal density, $\dot{m}_{nom}$ the nominal mass flow and $n_{channels}$ the number of parallel channels:

$$dp = \frac{K_f \dot{m}^2}{\rho} \tag{5}$$

$$K_f = \frac{dp_{nom} * LF * \rho_{nom}}{\left(\frac{\dot{m}_{nom}}{n_{channels}}\right)^2} \tag{6}$$

Lastly, the wall representing the interface of the water/steam side with the gas side is modeled as a 1D and flat domain, with a heat accumulation given by Eq. (7) (with m_{wall} being the total mass of the wall and c_p its heat capacity). The thermal resistance R_w is a function of the wall thickness, area and thermal conductivity.

$$\frac{m_{wall} c_p dT}{dt} = \frac{2(T_{wall,g} - T_{wall,steam/water})}{R_w} \tag{7}$$

The steam drum is modeled according to the formulations published previously [64], in which dynamic energy and mass balances are solved for the liquid and vapor volumes, accounting for bulk boiling and bulk condensation, respectively. Heat transfer through the drum wall and heat accumulation in the wall are neglected. Natural circulation in the drum-evaporator is modeled through an ideal height difference model with a pressure head such that the water flow through the downcomers and risers is ensured. Detailed descriptions of the drum dynamics can be found in the papers of Åström and Bell [65] and Eborn [61].

The steam turbine is described through a quasi-static model, which is a valid assumption given that its characteristic time is much shorter than the characteristic times associated with other components, such as the condensers or the furnace [66]. The turbine is modeled according to Stodola's law of cones [Eq. (8)], where $\dot{m}_{nom}$ is the nominal mass flow, $p_{i,nom}$ and $\rho_{i,nom}$ the pressure and density of the steam at turbine inlet, respectively and $p_{0,nom}$ the nominal outlet pressure.

$$K_t = \frac{\dot{m}_{nom}}{\sqrt{p_{i,nom}\rho_{i,nom}\left(1 - \left(\frac{p_{0,nom}}{p_{i,nom}}\right)^2\right)}} \tag{8}$$

Therefore, the effects of rotor dynamics, turbine casing and rotor inertia are not captured by the model. Consequently, dynamic interactions between the power grid and the steam cycle are here neglected. The dry isentropic efficiency of the turbine is assumed to be constant (0.89) throughout all the load levels investigated [67]. Lastly, a simple generator model is included to account for the mechanical shaft efficiency, which is assumed to be constant (0.98).

All the pumps present in the feedwater line are modeled as centrifugal pumps with mechanical efficiency of 0.98 and isentropic efficiency of 0.80. The computation of the flow is based on the quadratic flow characteristic, assuming a constant rotational speed. Control valves are modeled with linear opening flow characteristics. Thus, a flow coefficient determines the opening when compared to nominal conditions. The flow is assumed to be turbulent [68], and the accumulation of fluid and energy within the unit is neglected, i.e., the mass and energy balances are formulated as static.

The two condensers present in the reference unit are modeled as horizontal cylindrical vessels with immersed horizontal tubes, with the only difference being the cooling fluid (DH water and feedwater). At the bottom of the units, there is a hotwell in which the condensate is accumulated. A wall model such as that described in Section 4.2.1 [Eq. (7)] separates the condensing steam from the cooling fluid. The model assumes thermodynamic equilibrium between the liquid and vapor phases. Regarding the heat transfer, a correlation for condensing steam over horizontal tubes is used [62], whereas for the cooling media, a correlation for liquids similar to that depicted in Eq. (4) is used, albeit one that is based on the logarithmic average of the inlet and outlet temperatures and that is valid for both turbulent and laminar flows.

The deaerator (open feedwater heater) is modeled as a cylindrical open vessel, assuming thermodynamic equilibrium between the two phases. The model neglects heat transfer through the vessel walls.

Regulatory control loops present in the reference plant (see Section 2.3) are included in the model to ensure stable operation of the steam cycle. The PI controllers, the well-known Laplace-domain transfer function (G_c) of which is depicted in Eq. (9) (K_c is the controller gain and τ_I the integral time), are tuned according to the PID tuning rules published by Skogestad [69], and Table 8 lists the resulting tuning parameters of the regulatory control loops. For cascade loops, the slave controller (i.e., the internal, faster controller) is tuned first. Thereafter, the loop is closed and the master controller is tuned.

$$G_c(s) = K_c\left(1 + \frac{1}{\tau_I s}\right) \tag{9}$$

A similar approach is followed for implementing the supervisory control structures tested in this work (see Section 3.1). When tuning the supervisory controllers, the regulatory control layer is kept in closed

Table 8
Tuned parameters of the regulatory PI-controllers.

Controlled variable (CV)	Manipulated variable (MV)	K_c	τ_I
DHC level	Condensate valve opening	3,000	150
FWH level	Condensate valve opening	2,800	200
OFWH pressure	Steam valve opening	1	0.001
Drum level	FW valve	85	500
SH2 temperature	Attemperator water valve opening	−0.015	1
SH3 temperature	Attemperator water valve opening	−0.015	6

Table 9
Tuned parameters of the master supervisory PI-controllers (load controllers).

Control structure	K_c	τ_I
Turbine following	0.00040	200
Boiler following	0.00007	440
Floating pressure	0.00040	80
Hybrid	0.00007	440

loop with the same tuning parameters as listed in Table 8. Table 9 lists the tuning parameters of the master controllers (i.e., load controllers; see Figs. 2 and 3). Note that in all the control strategies in which the pressure is fixed, this loop is tuned and closed before the master controller.

4.3. Validation of the dynamic model

The integrated dynamic model presented here is validated against steady-state and transient operational data from the industrial reference unit presented in Section 2. As mentioned above, steady-state data at design load, i.e., 100 % load, were used for calibration (tuned parameters of the water-steam side are shown in Table A2 in Appendix A and of the in-furnace side in [29]), leaving the off-design datasets, i.e., 75 % and 50 % load, for the validation of the model. The steady-state validation of the integrated model is carried out by means of the absolute percentage error (*AP*) between the measured (x_m) and the simulated (x_s) process variables [see Eq. (10)].

$$AP = 100\frac{|x_m - x_s|}{x_m} \tag{10}$$

The results of the steady-state validation are shown in Table 10 (note that the measurement dataset for 75 % load lacked three signals), showing that all errors are <5 % with an average of 1.5 %, i.e., the model shows good agreement with the industrial data from off-design operation. Although the control structure is typically linked to the transient performance (such as that illustrated in Figs. 9 and 10 below), some assessment of the control structure can also be inferred from steady

Table 10
Steady-state validation of the main process variables simulated by the integrated process model (x_s) against the measured values (x_m) in the reference unit for different loads. AP, absolute percentage error.

Variable (unit)	100 % load (calibration)			75 % load (validation)			50 % load (validation)		
	x_m	x_s	AP (%)	x_m	x_s	AP (%)	x_m	x_s	AP (%)
P_{el} (MW)	19.86	19.60	1.31	–	15.23	–	9.08	9.28	2.20
Q_{DH} (MW)	56.88	54.18	4.98	–	42.29	–	28.91	28.49	1.45
F_{steam} (kg/s)	28.57	27.46	4.04	21.02	21.28	1.24	13.90	13.94	0.29
$T_{in,T}$ (°C)	494	493	0.17	494	491	0.55	496	492	0.81
$T_{DH,out}$ (°C)	90	92	2.56	–	90	–	84	84	0.11
P_{drum} (bar)	72.00	70.54	2.03	69.40	69.08	0.46	68.40	67.89	0.75

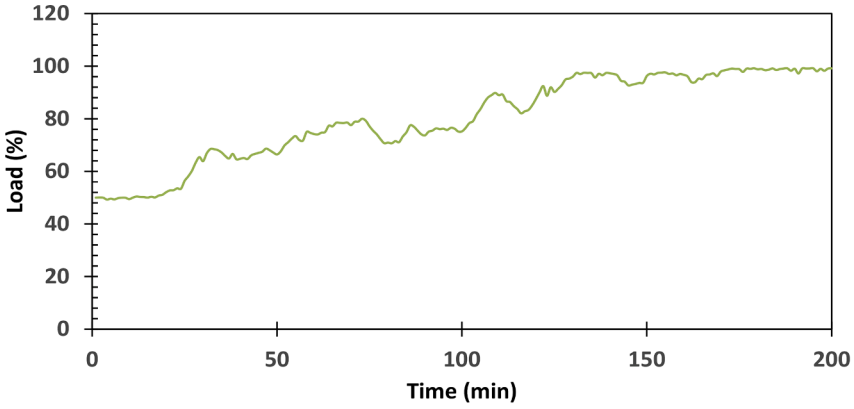

a) Thermal input load (%)

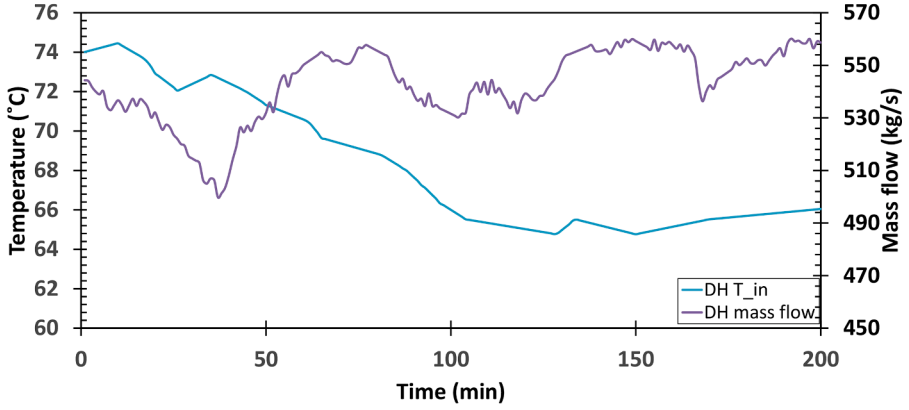

b) DH inlet temperature and mass flow

Fig. 9. Input trajectories to the model for transient operation validation.

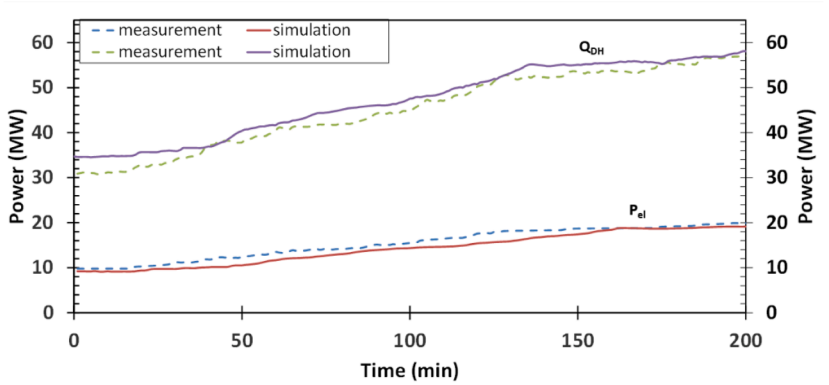

a) Generated district heating and electrical power (Q_{DH} and P_{el} respectively)

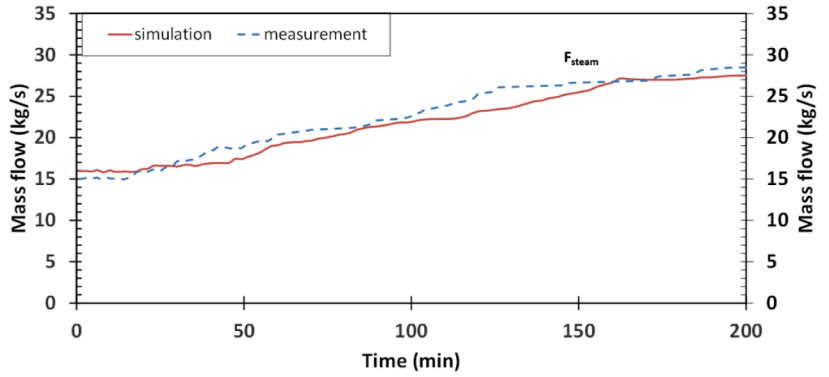

b) Live steam mass flow (F_{steam})

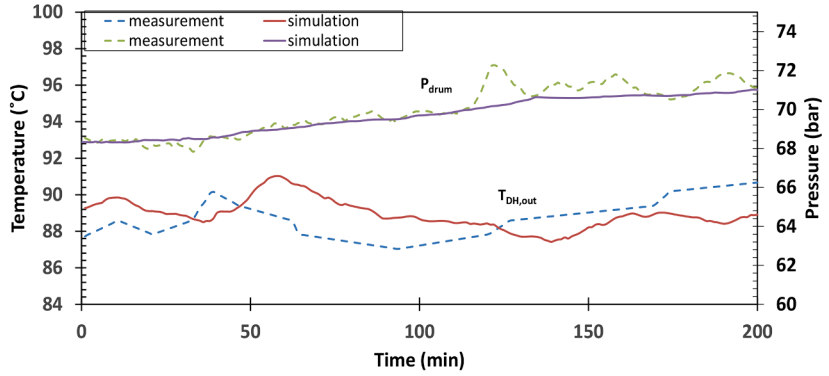

c) Drum pressure and district heating outlet temperature (P_{Drum} and $T_{DH,out}$ respectively).

Fig. 10. Transient validation of the main process variables when comparing the simulated and measured trajectories over a 3-h load increase.

state analysis. In relation to this, when resembling the control structure of an industrial plant, [17] two aspects of special importance are: (i) the achievement of stability, and (ii) the good agreement with the steady state values measured in the industrial facility. Regarding these two, (i) the control layer model attains stable solutions for all off-design operational points tested, and (ii) the steady states reached by the model shows an average error of 1.5 % as compared to measured values, as shown in Table 10. Thus, the model can satisfactorily predict steady-state operation within the operational window of interest in this work.

Validation of the transient performance of the model is performed by comparing the integrated model output with measurements taken over 3 h of operation during a load change from 50 % to 100 % load. Fig. 9 shows the transient input values to the model (the original time resolution was 1 min and it was interpolated to yield a resolution of 1 s). Note that this dataset was used for validation of the in-furnace dynamic model in [29], with the DH inlet mass flow and temperature (Fig. 9b) being the new inputs added for validation of the integrated process model. The set-point (SP) of the live steam pressure was fixed to the design value (67 bar) according to the operational strategy of the reference plant.

Fig. 10 compares the simulated and measured transient values of the main process variables used for model validation: power generation, P_{el}; live steam mass flow, F_{steam}; DH production, Q_{DH}; DH outlet temperature, $T_{DH,out}$; and drum pressure, P_{drum}. For each of these variables, the mean and maximum error values (calculated as AP) over the 200 min of the simulated period are shown in Table 11. While all the average error values are <6 %, the maximum errors observed in the electricity and DH production are 15 % and 11 % respectively. According to the transient trajectories plotted in Fig. 10, the model describes fairly well the transients of industrial operation, especially when it comes to predicting the electricity and DH generation as well as the live steam flow produced in the boiler. The reference data for the drum pressure exhibit some oscillations for some minutes that the model cannot predict, which is most likely due to differences in controller tuning procedures between the

Table 11
Mean and maximum errors (AP, absolute percentage error) over the 200 min period used for transient validation of the model.

Variable (unit)	Mean AP (%)	Maximum AP (%)
Q_{DH} (MW)	4.31	11.02
P_{el} (MW)	5.35	15.57
F_{steam} (kg/s)	4.65	9.87
P_{drum} (bar)	0.51	2.95
$T_{DH,out}$ (°C)	1.39	3.15

Table 12
RGA matrix of the 3 × 3 MV-CV system. Green cells represent the best pairing alternatives and orange cells indicate the pairings of turbine-following and sliding pressure strategies.

		MV		
		Q_{comb}	$Valve_{steam}$	F_{DSH}
CV	P_{el}	0.9721	0.0094	0.0185
	P_{steam}	0.0177	0.9814	0.0009
	T_{steam}	0.0102	0.0092	0.9806

industrial site and the model. Other discrepancies observed in, for instance, the outlet DH temperature, may be attributed to the fact that some design data required to model the plant were not available to the authors, so some assumptions were made (such as the residence time of the condensate in the hotwell or the characteristic curve of some pumps, among others).

In conclusion, based on the results presented previously [29] and in the present section, it can be stated that the integrated furnace-water/steam side dynamic model presented is capable of predicting the dynamic behaviors of industrial FBC-CHP plants with sufficient accuracy for the scope of this study, i.e., the analysis of the inherent and controlled dynamics of industrial-sized FBC-CHP plants.

5. Results and discussion

5.1. Relative gain analysis

The computed RGA matrix is shown in Table 12. The system studied is 3 × 3 and as such allows for six possible control structures (i.e., combination of MV-CV pairings). However, it can be seen in Table 12 (green cells) that only one structure provides a low degree of loop interactions (i.e., all RGA elements close to 1), i.e., controlling the generated electrical power with the combustion load, the live steam pressure with the main control valve opening, and the superheated steam temperature with the DSH water flow. These pairings correspond to turbine-following control (see Section 3.1.1). The remainder of the MV-CV connections give RGA elements close to 0, a sign of poor controllability [70]. Notably, among the structures showing poor controllability are both the well-established boiler-following control (see Section 3.1.2) and the sliding pressure control (Section 3.1.2.2), in which the electrical power is controlled by opening the steam valve and the steam pressure is controlled by the combustion load (orange cells in Table 12). The poor performances of these strategies in the RGA are explained by the fact that the valve opening only has a temporary effect on the power produced, due to the changes in pressure and mass flow, since the new steady-state reached after the transient effects is similar to that seen with the former valve opening. The only way to modify the steady-state pressure and flow (and, thereby, the electrical power) is through manipulating the energy added to the system, i.e., the combustion load. Thus, it can be concluded that the steady-state effect of the steam valve opening on the power generated is negligible, and that the only MV that can effectively change the levels of heat and power produced is the combustion load. Similar effects have been observed previously [20,32].

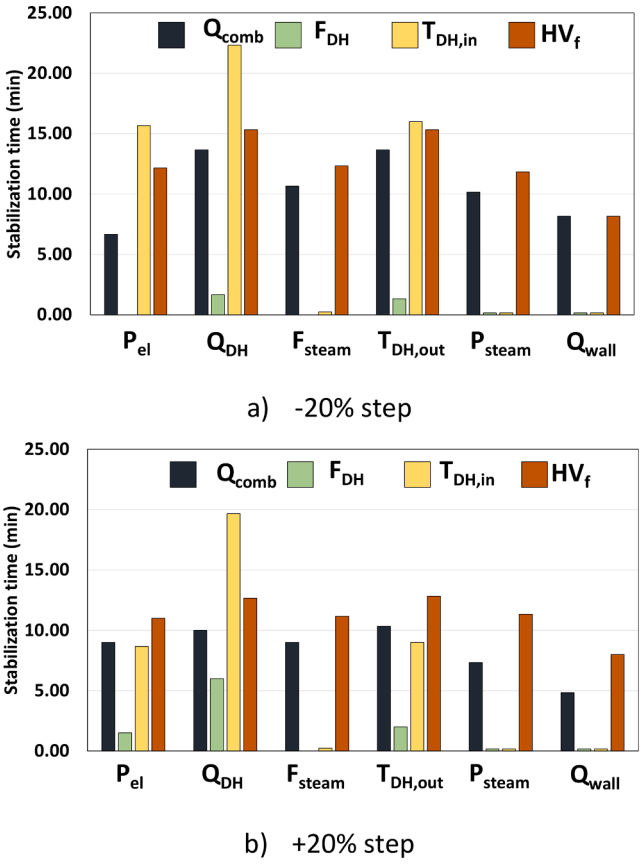

Fig. 11. Computed open-loop stabilization times for the main process variables for different process disturbances, i.e., step-changes in combustion load Q_{comb}, live steam mass flow F_{DH}, inlet district heating temperature $T_{DH,in}$, and heating value of the fuel HV_f (listed in Table 4).

5.2. Dynamic behavior of the reference plant

Below, we explore the dynamic behavior of the reference FBC-CHP plant. First, the uncontrolled dynamics of the system are computed in an open-loop analysis. Second, the control strategies described in Section 3.1 are tested in the integrated dynamic model for the variable ramping rate scenarios defined in Section 3.4. Third, the capabilities of the plant to achieve temporary overload by making use of the turbine bypass are evaluated.

5.2.1. Open-loop analysis

The computed stabilization times (in minutes) of the open-loop analysis performed when the plant is running at 80 % load are plotted in Fig. 11 for the six process variables monitored during the simulations. It is clear that for a step-change upwards or downwards (±20 %) for all of the investigated disturbances (Table 4), all the stabilization times are <25 min. In the water/steam side, the live steam pressure and mass flow are the variables that reach stabilization the fastest, with an average of 5 min, owing to the fact that pressure waves travel at the speed of sound in the fluid. This is in contrast to the velocity of the fluid in the pipe whereby the temperature is propagated in a plug flow model, thereby yielding faster stabilization times. The generated power stabilizes slightly more slowly (average stabilization time of 8 min), whereas the outlet DH temperature and the heat load in the DH condenser yield the slowest times for stabilization, averaging 10 min and 13 min, respectively, for the cases investigated. It is important to highlight that the times computed for the live steam variables can be related to the stabilization time of the in-furnace heat transfer Q_{wall} (5–10 min in this work; see [29] for details). This confirms the usefulness of modeling the

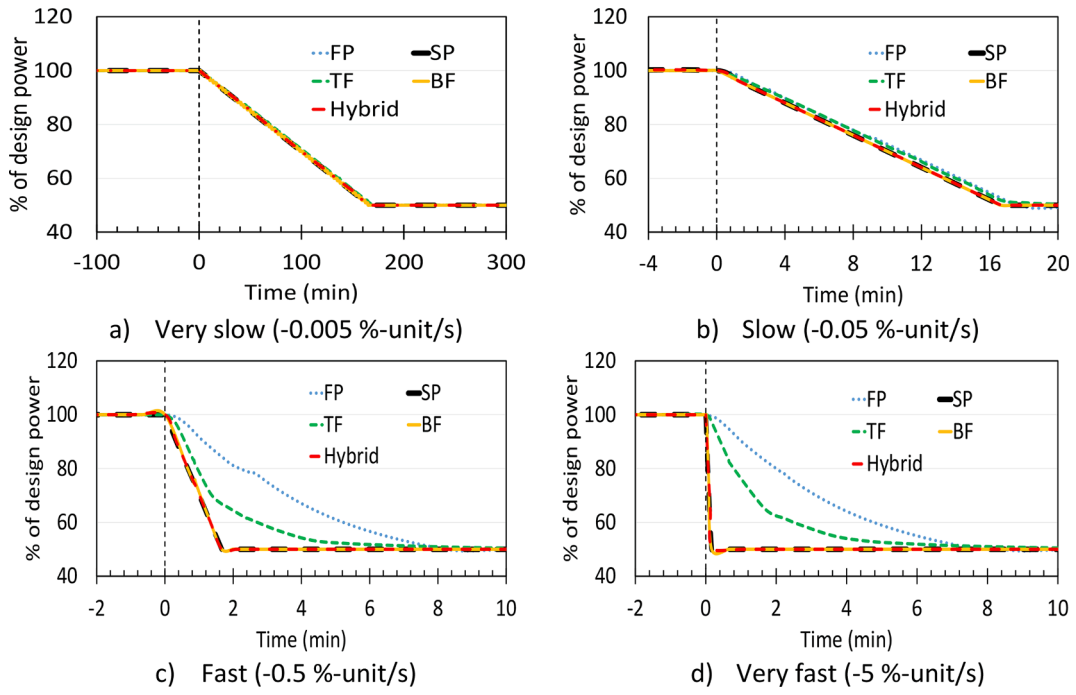

Fig. 12. Electrical power output responses (in % of the design electrical power) compared to the load set point (SP) for Scenario I under different control structures and ramping rates. BF, Boiler-following; FP, floating pressure; TF, turbine-following.

in-furnace side for understanding and describing the live steam dynamics. The computed stabilization times also reveal that in the water/steam side, process equipment with steam-only inventories generally have faster dynamics that those in which liquid and steam coexist. The stabilization times listed in Fig. 11 show that the process response is the fastest for changes in the DH mass flow, which is in line with the results from a previous study [8]. Note that changes in the DH flow and temperature do not affect the live steam conditions, and the change observed in the generated power is caused by the variations in the condensing pressure. The disturbances linked to the in-furnace side cause the slowest responses in the system, with the stabilization times for changes in combustion load (Q_{comb}) and fuel heating value (HV_f) averaging 11 min and 13 min, respectively, across all six variables (both for the step-down case, i.e., Fig. 11a).

Differences in stabilization times between a step-change down and a step-change up are observed when comparing Fig. 11, a and b. The process tends to stabilize faster (15 % shorter stabilization times on average) when heat is added to the system, i.e., when the combustion load, fuel heating value and DH inlet temperature increase. This non-linearity has been reported in several studies that have investigated the inherent dynamics of various thermochemical processes (see for instance [57,71]), and is in agreement with the results obtained from the analysis of the in-furnace side [29]. In a previous study [18], it has been highlighted that the mechanism driving the load increase, i.e., the fuel conversion, is an order of magnitude faster than that leading the load reduction, i.e., the heat transfer to the waterwalls (as a consequence of the thermal inertia caused by the furnace solids).

When the same open-loop tests are simulated for the process running at 70 % load instead, all six process variables are found to stabilize more slowly than they do in the 80 % load case. This difference ranges from 9 % slower in the case of the DH outlet temperature up to 25 % slower for the generated electricity. This effect has been reported earlier for thermal power plants [8,29], and is caused by the decrease in flows that is intrinsic to partial-load operation, which inevitably increases the residence time of the fluid both in the gas and water/steam sides.

5.2.2. Variable ramping rate analysis

Fig. 12 shows the responses of the generated power (in percent of the design load, i.e., 100 %) for each of the supervisory control strategies and for all the cases simulated as part of Scenario I, i.e., when the power output is reduced from 100 to 50 %. It is evident that for the very slow and slow cases (*cf.* Table 7), all the strategies are capable of providing load changes at the same rate as the set-point (SP) is changed, with the exception of the floating pressure operation, which shows some delay and undershoot, reaching stabilization some 4 min after the SP. As shown in Fig. 12, most of the differences between the control strategies occur in the faster cases. It is observed that while the control strategies that manipulate the live steam control valve (BF and hybrid control strategies) provide very fast power output changes that follow the SP, those that manipulate the combustion load (FP and TF) are considerably slower. In both the fast and very fast cases, floating pressure operation shows the slowest response, with a rising time of 6 min and a stabilization time of 10 min. Turbine-following operation displays a faster rising time than FP (4 min) and a similar stabilization time (10 min). The differences between FP and TF observed in the fast and very fast cases are within expectations, since TF makes use of the steam control valve to correct the pressure deviations, which has a dynamic effect on the power production. Similar characteristics were observed in a previous study [20], while [16] has claimed that FP operation provides up to 50 % slower ramp rates than the BF and hybrid control strategies. The same reasoning applies when explaining how the BF and hybrid strategies yield the fastest (and similar) responses: the dynamic effect of the control valve uses the energy accumulated in the drum and steam lines to generate fast temporary changes in the steam pressure and mass flow, which quickly propagate to the turbine. If the combustion load is not changed subsequently, the new steady state reached would be similar to the previous one, according to what was observed in the RGA. It is the combination of the steam control valve and the combustion load that enables the quick and effective load changes plotted in Fig. 12.

Since the fast changes in power output reported in Fig. 12 occur due to the rapid dynamics of steam throttling, the live steam pressure is plotted in Fig. 13 for the fastest ramping rates under TF, BF and hybrid control operations. It is clear that the quick changes in power output

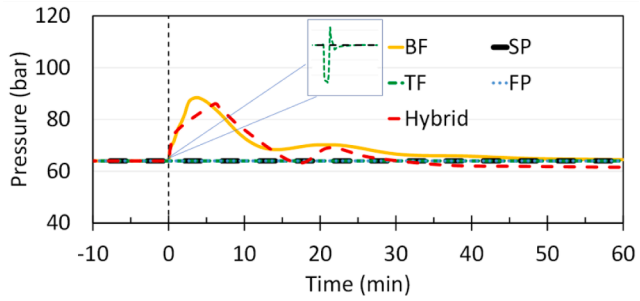

Fig. 13. Live steam pressure prior to the master control valve when compared to the set point (SP), for Scenario I – Very fast (0.005 %-unit/s). Boiler-following, BF, floating pressure. FP; turbine-following, TF.

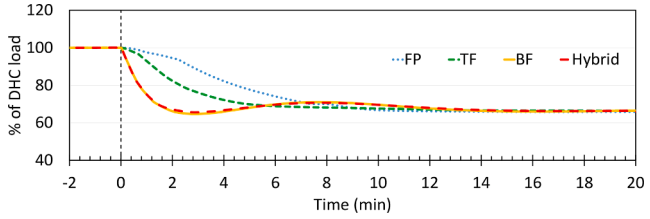

Fig. 14. District heating (DH) production (as % of the design load) for) for Scenario I – Very fast (0.005 %-unit/s)-under different control strategies. BF, Boiler-following; FP, floating pressure; TF, turbine-following.

provided by the BF and hybrid control operations occur at the expense of substantial steam throttling when the control valve is suddenly closed. The overshoot in the pressure trajectory is +30 % for the BF case versus ±0.01 % for the TF strategy. In the case of BF operation (and similarly in hybrid control operation), the temporary increase in the live steam pressure is directly linked to exergy losses and, therefore, the loss of available work, with a negative impact on process efficiency during the transient. Furthermore, once the new steady-state is reached, the partial closure of the control valve is also linked to reductions in enthalpy and power-to-heat ratio [19]. The complete opposite situation occurs during FP operation, whereby the valve remains fully open during all the operational window simulated here. Thus, even though it provides the slowest response due to the longer characteristic times of the in-furnace side, it is the strategy that maximizes process efficiency during both transient and partial-load operation. TF operation represents an intermediate case, with higher process efficiency during transient operation than is achieved with BF or hybrid control (since the temporary closure of the control valve is less drastic). These results highlight the tradeoff that exists between flexibility and efficiency, as well as the operational constraints associated with flexibilization, both of which topics are explored further in Section 5.3. Regarding the question as to whether the live steam pressure should be controlled, it can be concluded from these results that controlling the pressure gives the fastest power response (except for boiler-following operation), although leaving the live steam valve opened enhances process efficiency and controllability. With regards to the live steam temperature, very few variations are found due to the fact that it is a controlled variable under all the tested strategies, with measured undershoots of <5 %.

Conclusions analogous to those related to the power generation can be drawn regarding the DH production. For simplicity, only the very fast rate of Scenario I is plotted in Fig. 14, where again the operation with FP shows the slowest response and BF and hybrid control strategies show the fastest responses. For the case shown, FP displays a rising time of 7 min and a stabilization time of 10 min, as compared to the 3 min and 10 min, respectively, for the hybrid and BF control strategies. Note that the DHC has been simulated with a constant mass flow and variable outlet temperature, since this is a conventional way of operating DH networks in order to avoid water hammering issues (although the operational dataset used for model validation presented some flow fluctuations; see Fig. 9).

Similar findings to those presented above for Scenario I were obtained for Scenario II (50−>40 % load) and, therefore, these results are not included here. In general, all the rising and stabilization times are slightly shorter than in Scenario I, which can be attributed to the smaller absolute change in load of Scenario II [29]. Similarly, the pressure overshoots for hybrid and BF operations are decreased with respect to Scenario I.

5.2.3. *Other strategies – Turbine bypass*

Fig. 15 shows the responses of the simulated turbine bypass after the bypass valve is opened to allow the flow of 3, 5 and 7 kg/s of live steam when the boiler is running steadily at 50 % load. The rise time of the electrical power output (Fig. 15a) responses lies between 25 s and 60 s, and it increases in line with the bypass flow. It can be seen that the response of the DH output (Fig. 15b) is slower than that of the electrical output, with stabilization times in the range of 6–8 min. When the valve is closed (Fig. 15, c and d) the power is increased with rise times of around 1 min, regardless of the magnitude of the bypass flow. These

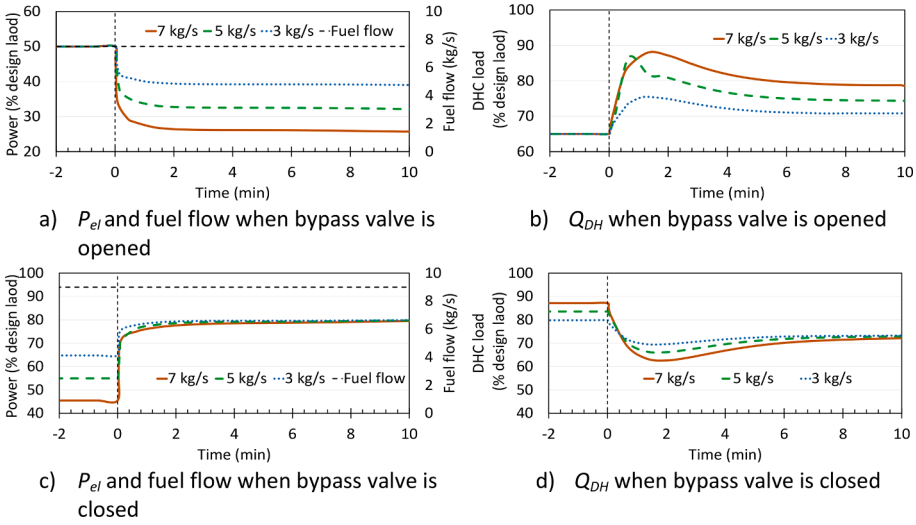

Fig. 15. For different bypassed flows, simulated responses of the generated electrical power and district heating (P_{el} and Q_{DH} respectively) when the bypass valve is opened (a and b) and closed (c and d).

results are in line with published work [54].

The fuel flow over the bypass opening has been added in Fig. 15, a and c, and, as expected, it remains constant. This is important for emissions control, combustion efficiency and intraday trading, as discussed further in Section 5.3. Another conclusion that can be drawn from Fig. 15 is that turbine bypass allows for the decoupling of the heat and power productions, effectively increasing the plant product flexibility [11]. It can also be concluded from Fig. 15 that operation with turbine bypass expands the operational boundaries of the plant, allowing reduction of the minimum power load without altering the combustion process.

5.3. Practical implications

The validity of the simulation results presented in Section 5.2 and their practical implications for the flexibility of biomass-based FBC-CHP plants are discussed in this section.

First of all, the results from the variable ramping rate (VRR) highlight the importance of the control strategy selected when it comes to providing load changes. The results of this work demonstrate that control strategies using the turbine control valve can provide large changes in load (magnitude of around 10 MW_e) with response times of 30–60 s. This is achieved by making use of the throttling reserve to store some energy in the steam generator surfaces, allowing the plant to provide fast load changes while avoiding the delay and inertia of the in-furnace side. However, throttling is by definition a purely dissipative process (isentropic) above the ambient temperature, decreasing the fluid enthalpy without the production of useful work. It has been shown that the faster the ramping rate, the more energy is dissipated through throttling, given that the control valve needs to close more swiftly.

In addition, other operational constraints must be considered when assessing the capabilities for very fast load changes. For instance, the reference plant considered in this work has a high-pressure alarm in the drum for steam pressures above 80 bar, which for the boiler-following response (Fig. 13) would be triggered for the load change simulated for Scenario I. Moreover, thermal stresses in the turbine and thick-walled components of the boiler and condensers are amplified when the steam pressure and temperature vary substantially and frequently. In contrast, in floating pressure operation, the live steam valve remains unaltered, which combined with the live steam temperature control makes the steam entering the turbine to be at a constant temperature at all loads.

Too-rapid load changes can cause undesired emissions from the furnace (see [29]). Thus, although physically feasible with the right control strategy, detailed optimization studies are needed to determine the profit loss and gain related to providing load changes in these short timeframes on a regular basis, for instance, to meet a need for primary control reserve (in most European markets characterized by response times in the order of 30 s). Note that the dynamics of other components not included in the present model, such as the fuel handling and feeding systems, would also play a role in the total transient capabilities of the plant. Moreover, sometimes the bottleneck of the plant lays on the regulatory control layer, as it is tuned so slow that there is not a good timescale separation between the layers, thereby creating potential instabilities or odd transients. Furthermore, slow tuning of the regulatory control layer can lead to noticeable undershoots in steam temperature when the load is quickly ramped downwards. Lastly, it is worth mentioning that there are a number of advanced control strategies (e.g., integrated, coordinated or parallel control) which, being extensions of the ones presented here, have not been included in the present study. Nevertheless, they could partially contribute to solving some of the operational issues identified here, e.g., the pressure overshoots.

The addition of a high-pressure steam extraction that bypasses the turbine is shown to resolve partially the problems of emissions and thermal stresses identified above. First, it allows the provision of fast changes in power (with response times of around 1 min for the cases investigated) without the operational problems associated with steam throttling. Furthermore, the fuel supply can remain constant, which could solve the issues linked to undesired emissions. Thus, appropriate design and implementation of the turbine bypass could enable intraday and balancing trading capabilities, as well as the reduction of minimum load while maintaining DH generation. The latter is of particular interest when electricity prices are low but the demand for DH remains high.

The implications that operating FBC-CHP plants to enable fast changes in power output have for the production of DH can also be assessed. The DH networks are characterized by slow (and often predictable) demand changes, as well as the high thermal inertia seen in conventional DH systems, which dampens the oscillations connected to DH disturbances. Thus, the DH flow and temperatures could be assumed to be quasi-static for the timeframe investigated. Furthermore, there is the possibility to add thermal energy storage to the DH system, so as to buffer the variations caused by the load-change scenarios investigated. This would also allow the heat and power production outputs of the plant to be dispatched based on electricity prices, rather than on DH demand, and would facilitate shifting heat production in time to remove peak heat-only boiler units of the DH system that may run on fossil fuels.

6. Conclusions

The present work entails an analysis of the inherent and controlled transient operation capabilities of fluidized bed combustion plants for combined heat and power production. A model of the in-furnace side of fluidized bed combustors is integrated into a dynamic process model of the water/steam side. After validation with industrial operational data, the model is applied to perform both a relative gain analysis and dynamic analysis, in which the inherent dynamics of the process as well as the performances of different control structures identified from the literature are evaluated.

Based on the results obtained, the main conclusions of the work are summarized as follows:

- While most of the literature has often assumed the water-steam side to be the limiting the transient operation of fluidized bed combustion plants, the present paper shows that the in-furnace and water-steam sides of fluidized bed combustion plants have inherent characteristic times in the same order of magnitude. Thus, modeling of the in-furnace side cannot be disregarded in dynamic analyses at plant level.
- The use of control and operational strategies such as turbine bypass can enhance the operational and product flexibility of fluidized bed combustion plants for combined heat and power production, enabling temporary over-underload performance as well as providing load changes at constant combustion load, i.e., avoiding the delay associated with the in-furnace side. Yet, a more detailed assessment of component lifetime versus revenue is needed in order to extract further conclusions.

The results and conclusions derived from this work should be of importance when assessing the operational capabilities of fluidized bed combustion plants for combined heat and power production when they are operated to provide fast load changes. Nevertheless, further research accounting for the thermal stresses and lifetimes of key power plant components is required to construct a comprehensive economic picture of the implications of flexible operation.

Funding

This work was supported by the Swedish Energy Agency (project 46459-1, “Cost-effective and flexible polygeneration units for maximized plant use”).

Declaration of Competing Interest

The authors declare that they have no known competing financial interests or personal relationships that could have appeared to influence the work reported in this paper.

Data availability

The authors do not have permission to share data.

Appendix A. Water/steam side model

See Tables A1 and A2.

Table A1
Equations used to model the different components of the water/steam side model.

Component	Formulation/magnitude	Equation	Ref
Economizers and Superheaters	Heat transfer gas side	$\alpha = C\frac{F_a Nu_0 \lambda}{d_{hyd}}$	[62]
	Energy balance gas side	$\dot{m}(h_{out} - h_{in}) = \alpha A(T_{gas} - T_{wall})$	–
	Mass balance gas side	$\frac{d\dot{m}}{dt} = 0$	[72]
	Heat transfer water/steam side	$\alpha = C\frac{Nu_0 \lambda}{d_{hyd}}$	[62]
	Mass balance water/steam side	$\frac{d\dot{m}}{dt} = \dot{m}_{out} - \dot{m}_{in}$	–
	Pressure drops	$dp = \frac{K_f \dot{m}^2}{\rho}$ $K_f = \frac{dp_{nom} * LF * \rho_{nom}}{\left(\frac{\dot{m}_{nom}}{n_{channels}}\right)^2}$	[8,73]
	Walls connecting pipes	$R_w = \frac{s/\lambda}{A}$ $\frac{m_{wall} c_p dT}{dt} = \frac{2(T_{wall,g} - T_{wall,steam/water})}{R_w}$	–
Evaporator tubes	Heat transfer water side	$\alpha_{tp} = \psi \alpha_L$ $\psi = f(Co, Bo)$ $\alpha_L = 0.023 Re^{0.8} Pr_L^{0.4} (\frac{\lambda_L}{d_{hyd}})$ $Co = \left[\frac{1-x}{x}\right]^{0.8} \left[\frac{\rho_v}{\rho_L}\right]^{0.8}$ $Bo = \frac{q}{G \bullet h_{vap}}$	[58]
	Pressure drops	$dp = \frac{K_f \dot{m}^2}{\rho} = 0$ $K_f = \frac{dp_{nom} * LF * \rho_{nom}}{\left(\frac{\dot{m}_{nom}}{n_{channels}}\right)^2}$	[8,73]
	Walls connecting pipes	$R_w = \frac{s/\lambda}{A}$ $\frac{m_{wall} c_p dT}{dt} = \frac{2(T_{wall,g} - T_{wall,steam/water})}{R_w}$	–
Turbine	Stodola Law of cones for off-design conditions	$K_t = \frac{\dot{m}_n}{\sqrt{p_{i,n}\rho_{i,n}\left(1 - \left(\frac{p_{0,n}}{p_{i,n}}\right)^2\right)}}$	[74]
	Dry isentropic efficiency degradation	$\eta_{is,wet} = \eta_{is,dry} - \beta(1-x)$	[75]
	Energy balance	$h_{out} = h_{in} - \eta_{is}(h_{in} - h_{is})$	–
	Generator	$P_{el} - \eta_{mech}\dot{m}(h_{in} - h_{out})$	–
Condensers	Mass balance hot side	$\frac{d\dot{m}}{dt} = \dot{m}_{in} - \dot{m}_{out}$	–
	Heat transfer hot side	Correlation for film condensation over horizontal tube bundles $= f(Re, Pr, x, p, p_{crit}, d_{hyd})$	[62]
	Mass balance cold side	$\dot{m}_{in} = \dot{m}_{out}$	[8]
	Driving force heat transfer cold side	$\Delta T_{L,M} = \frac{T_{wall} - T_{in}}{T_{wall} - T_{out}}$	[62]
	Walls	$R_w = \frac{s/\lambda}{A}$ $\frac{m_{wall} c_p dT}{dt} = \frac{2(T_{wall,g} - T_{wall,steam/water})}{R_w}$	–
Open feedwater heater	Energy balance	$\frac{dE}{dt} = \dot{m}_c h_c + \dot{m}_{st} h_s - \dot{m}_{fw} h_{fw}$	–
	Mass balance	$\frac{d\dot{m}}{dt} = \dot{m}_c + \dot{m}_{st} - \dot{m}_{fw}$	–
Pumps	Volume flow rate	$\dot{V}_2 = \dot{V}_1 \left(\frac{N_2}{N_1}\right)\left(\frac{d_2}{d_1}\right)$	–
	Total head	$H_2 = H_1 \left(\frac{N_2}{N_1}\right)^2 \left(\frac{d_2}{d_1}\right)^2$	–
Valves	Linear valve characteristic	$\dot{m} = \theta \bullet C_v \bullet \frac{\dot{m}_{nom}}{\sqrt{\rho \bullet dp_{nom}}} \sqrt{\frac{p_{in} - p_{out}}{dp_{nom}}}$	[68]

Table A2
Calibration factors used to match steady-state operational data at 100% load.

Component	Calibration Factor	
	Gas side	Water-steam side
ECO 1	1.00	0.05
ECO 2	1.00	0.05
ECO 3	1.00	0.05
SH1	10.00	0.14
SH2	0.50	1.30
SH3	1.00	0.12
Evaporator tubes	–	2.00

References

[1] International Energy Agency, Renewables 2019, 2019. <https://webstore.iea.org/renewables-2019>.
[2] International Renewable Energy Agency, IRENA (2019), Global Energy Transformation: A Roadmap to 2050, 2019. <https://www.irena.org/publications/2019/Apr/Global-energy-transformation-A-roadmap-to-2050-2019Edition>.
[3] L. Göransson, F. Johnsson, A comparison of variation management strategies for wind power integration in different electricity system contexts, Wind Energy. 21 (2018) 837–854, https://doi.org/10.1002/we.2198.
[4] R. Lund, B.V. Mathiesen, Large combined heat and power plants in sustainable energy systems, Appl. Energy. 142 (2015) 389–395, https://doi.org/10.1016/j.apenergy.2015.01.013.
[5] IEA, Harnessing variable renewables: a guide to the balancing challenge, 2011.
[6] V. Johansson, M. Lehtveer, L. Göransson, Biomass in the electricity system : A complement to variable renewables or a source of negative emissions? Energy. 168 (2019) 532–541, https://doi.org/10.1016/j.energy.2018.11.112.
[7] G. Bergendahl, Investeringar i kraftvärme – Ekonomiska och miljömässiga fördelar, Gothenburg (2008). https://gupea.ub.gu.se/bitstream/2077/9629/1/2008-413.pdf.
[8] J. Beiron, R.M. Montañés, F. Normann, F. Johnsson, Dynamic modeling for assessment of steam cycle operation in waste-fired combined heat and power plants absolute percentage deviation, Energy Convers. Manag. 198 (2019), 111926, https://doi.org/10.1016/j.enconman.2019.111926.
[9] E. Mollenhauer, A. Christidis, G. Tsatsaronis, Increasing the Flexibility of Combined Heat and Power Plants With Heat Pumps and Thermal Energy Storage 140 (2018) 1–8. <https://doi.org/10.1115/1.4038461>.
[10] M. Richter, G. Oeljeklaus, K. Görner, Improving the load flexibility of coal-fired power plants by the integration of a thermal energy storage, Appl. Energy. 236 (2019) 607–621, https://doi.org/10.1016/j.apenergy.2018.11.099.
[11] J. Beiron, R. M. Montañés, F. Normann, F. Johnsson, Combined heat and power operational modes for increased product flexibility in a waste incineration plant 202 (2020). <https://doi.org/10.1016/j.energy.2020.117696>.
[12] S. Kahlert, Investigation of different operation strategies to provide balance energy with an industrial combined heat and power plant using dynamic, Simulation 139 (2017) 1–8, https://doi.org/10.1115/1.4034184.
[13] Y. Gao, Y. Hu, D. Zeng, J. Liu, F. Chen, Modeling and control of a combined heat and power unit with two-stage bypass 11 (2018) 1–20. https://doi.org/10.3390/en11061395.
[14] A.D. Zareh, R.K. Saray, S. Mirmasoumi, K. Bahlouli, Extensive thermodynamic and economic analysis of the cogeneration of heat and power system fueled by the blend of natural gas and biogas, Energy Convers. Manag. 164 (2018) 329–343, https://doi.org/10.1016/j.enconman.2018.03.003.
[15] C.A. Salman, C.B. Omer, Process modelling and simulation of waste gasification-based flexible polygeneration facilities for power, heat and biofuels production, Enegies. 13 (16) (2020). https://doi.org/10.3390/en13164264.
[16] S. Stultz, J. Kitto, Controls for Fossil Fuel-Fired Steam Generating Plants, in: Steam Its Gener. Use, The Babcok and Wilcox Company, 2005: pp. 41–1, 41–21. <https://doi.org/10.1515/9783110214130.489>.
[17] S. Skogestad, I. Postlethwaite, Multivariable Feedback Control, Wiley, Analysis and design, 2006.
[18] R. Kehlhofer, et al., Combined Gas and Steam Power Plants, third ed.,, PennWell, 2009.
[19] K. Jonshagen, M. Genrup, Improved load control for a steam cycle combined heat and power plant, Energy. 35 (2010) 1694–1700, https://doi.org/10.1016/j.energy.2009.12.019.
[20] C. Zotica, L.O. Nord, J. Kovács, S. Skogestad, Optimal operation and control of heat to power cycles: a new perspective from a systematic plantwide control approach, Comput. Chem. Eng. 141 (2020), 106995, https://doi.org/10.1016/j.compchemeng.2020.106995.
[21] Y. Zhao, M. Liu, C. Wang, X. Li, D. Chong, J. Yan, Increasing operational flexibility of supercritical coal-fired power plants by regulating thermal system configuration during transient processes, Appl. Energy. 228 (2018) 2375–2386, https://doi.org/10.1016/j.apenergy.2018.07.070.
[22] Y. Zhao, C. Wang, M. Liu, D. Chong, J. Yan, Improving operational flexibility by regulating extraction steam of high-pressure heaters on a 660 MW supercritical coal-fired power plant: a dynamic simulation, Appl. Energy. 212 (2018) 1295–1309, https://doi.org/10.1016/j.apenergy.2018.01.017.
[23] F. Alobaid, N. Mertens, R. Starkloff, T. Lanz, C. Heinze, B. Epple, Progress in dynamic simulation of thermal power plants, Prog. Energy Combust. Sci. 59 (2017) 79–162, https://doi.org/10.1016/j.pecs.2016.11.001.
[24] I. Avagianos, D. Rakopoulos, S. Karellas, E. Kakaras, Review of process modeling of solid-fuel thermal power plants for flexible and off-design operation, Energies. 13 (2020). https://doi.org/10.3390/en13246587.
[25] J. Beiron, R.M. Montañés, F. Normann, F. Johnsson, Flexible operation of a combined cycle cogeneration plant – a techno-economic assessment, Appl. Energy. 278 (2020), 115630, https://doi.org/10.1016/j.apenergy.2020.115630.
[26] T. Nussbaumer, Combustion and co-combustion of biomass : fundamentals, technologies, and primary measures for emission reduction †, Energy Fuels. 17 (2003) 1510–1521, https://doi.org/10.1021/ef030031q.
[27] I. Obernberger, Decentralized biomass combustion : state of the art and future development *, Biomass Bioenergy. 14 (1998) 33–56.
[28] C. Yin, L.A. Rosendahl, S.K. Kær, Grate-firing of biomass for heat and power production, Prog. Energy Combust. Sci. 34 (2008) 725–754, https://doi.org/10.1016/j.pecs.2008.05.002.
[29] G. Martinez Castilla, R.M. Montañés, D. Pallares, F. Johnsson, Dynamic modeling of the reactive side in large-scale fluidized bed boilers, Ind. Eng. Chem. Res. 60 (2021) 3936–3956, https://doi.org/10.1021/acs.iecr.0c06278.
[30] M. Gao, F. Hong, J. Liu, Investigation on energy storage and quick load change control of subcritical circulating fluidized bed boiler units, Appl. Energy. 185 (2017) 463–471, https://doi.org/10.1016/j.apenergy.2016.10.140.
[31] G. Martinez Castilla, R.M. Montañés, D. Pallarès, F. Johnsson, Comparison of the Transient Behaviors of Bubbling and Circulating Fluidized Bed Combustors, Heat Transf. Eng. (2022) 1–14 (in press). <https://doi.org/10.1080/01457632.2022.2059214>.
[32] M. Hultgren, E. Ikonen, J. Kova, Once-through Circulating Fluidized Bed Boiler Control Design with the Dynamic Relative Gain Array and Partial Relative Gain, 2017. <https://doi.org/10.1021/acs.iecr.7b03259>.
[33] M. Hultgren, E. Ikonen, Integrated control and process design for improved load changes in fluidized bed boiler steam path 199 (2019) 164–178. <https://doi.org/10.1016/j.ces.2019.01.025>.
[34] N. Zimmerman, K. Kyprianidis, C.-F. Lindberg, Waste fuel combustion: dynamic modeling and control, Processes. 6 (2018) 222, https://doi.org/10.3390/pr6110222.
[35] H. Zhang, M. Gao, F. Hong, J. Liu, X. Wang, Control-oriented modelling and investigation on quick load change control of subcritical circulating fluidized bed unit, Appl. Therm. Eng. 163 (2019), 114420, https://doi.org/10.1016/j.applthermaleng.2019.114420.
[36] S. Kim, S. Choi, T. Song, Dynamic simulation study of the steam temperature in a ultra-supercritical circulating fluidized bed boiler system, 2020. <https://doi.org/10.1177/0957650920915304>.
[37] S. Kim, S. Choi, J. Yang, Dynamic simulation of a circulating fluidized bed boiler system Part I : Description of the dynamic system and transient behavior of sub-models Dynamic simulation of a circulating fluidized bed boiler system Part I : Description of the dynamic system and, 2016. <https://doi.org/10.1007/s12206-016-1148-8>.
[38] D. Stefanitsis, A. Nesiadis, K. Koutita, Simulation of a CFB Boiler Integrated With a Thermal Energy Storage System During Transient Operation, 8 (2020) 1–14. <https://doi.org/10.3389/fenrg.2020.00169>.
[39] M. Zlatkovikj, V. Zaccaria, I. Aslanidou, K. Kyprianidis, Simulation study for comparison of control structures for BFB biomass boiler, in: 61st SIMS Conf. Simul. Model., Oulu, Finland, 2020.
[40] M. De Rosa, M. Carragher, D.P. Finn, Flexibility assessment of a combined heat-power system (CHP) with energy storage under real-time energy price market framework, Therm. Sci. Eng. Prog. 8 (2018) 426–438, https://doi.org/10.1016/j.tsep.2018.10.002.
[41] T. Takeshita, H. Aki, K. Kawajiri, M. Ishida, Assessment of utilization of combined heat and power systems to provide grid flexibility alongside variable renewable energy systems, Energy. 214 (2021), 118951, https://doi.org/10.1016/j.energy.2020.118951.
[42] K. Atsonios, A. Nesiadis, N. Detsios, K. Koutita, N. Nikolopoulos, P. Grammelis, Review on dynamic process modeling of gasification based biorefineries and bio-based heat & power plants, Fuel Process. Technol. 197 (2020), 106188, https://doi.org/10.1016/j.fuproc.2019.106188.
[43] J. Kjärstad, F. Johnsson, The European power plant infrastructure-presentation of the Chalmers energy infrastructure database with applications, Energy Policy. 35 (2007) 3643–3664, https://doi.org/10.1016/j.enpol.2006.12.032.
[44] E.M.B. Aske, S. Skogestad, Consistent inventory control, Ind. Eng. Chem. Res. 48 (2009) 10892–10902, https://doi.org/10.1021/ie801603j.
[45] G.E. Weber, W.M. Worek, Sliding pressure analysis using the second law, Heat Recover. Syst. CHP. 13 (1993) 253–260, https://doi.org/10.1016/0890-4332(93)90015-N.
[46] G. Klefenz, Automatic Control of Steam Power Plants, Bibliographisches Institut, 1986.
[47] C. Zhang, Y. Li, H. Wang, B.A.O. Zhang, F.E.I. Xie, Y.U. Huang, Selection of the optimal steam pressure for coal-fired power units, ICMLC, 2005, pp. 1835–1838.
[48] S. Sengupta, A. Datta, S. Duttagupta, Exergy analysis of a coal-based 210 MW thermal power plant, Internatinal J. Energy Res. (2007) 14–28, https://doi.org/10.1002/er.
[49] M.G. Jacobsen, S. Skogestad, Active constraint regions for economically optimal operation of distillation columns, Sep. Div. - Core Program. Top. 2011 AIChE Annu. Meet. 1 (2011) 474–475.
[50] E. Bristol, On a new measure of interaction for multivariable process control, IEEE Trans. Autom. Control. 11 (1) (1966) 133–134.

[51] M.A. Gonzalez-Salazar, T. Kirsten, L. Prchlik, Review of the operational flexibility and emissions of gas- and coal-fired power plants in a future with growing renewables, Renew. Sustain. Energy Rev. 82 (2018) 1497–1513, https://doi.org/10.1016/j.rser.2017.05.278.
[52] M. Thern, K. Jordal, M. Genrup, Temporary CO 2 capture shut down: implications on low pressure steam turbine design and efficiency, Energy Proc. 51 (2014) 14–23, https://doi.org/10.1016/j.egypro.2014.07.002.
[53] D. Seborg, T. Edgar, D. Mellichamp, F. Doyle, Process Dynamics and Control, John Wiley & Sons, 2011.
[54] J. Beiron, R.M. Montañés, F. Normann, Operational flexibility of combined heat and power plant with steam extraction regulation, in: Proc. 11th Int. Conf. Appl. Energy, Västerås, 2019, pp. 1–4.
[55] D. Systemes, Dymola Systems Engineering, 2021, 2021. <https://www.3ds.com/products-services/catia/products/dymola/> (Accessed June 15, 2021).
[56] Modelica Association, Modelica and the Modelica Association, 1996. <https://www.modelica.org/> (Accessed May 14, 2021).
[57] R.M. Montañés, S. GarÐarsdóttir, F. Normann, F. Johnsson, L.O. Nord, Demonstrating load-change transient performance of a commercial-scale natural gas combined cycle power plant with post-combustion CO2capture, Int. J. Greenh. Gas Control. 63 (2017) 158–174, https://doi.org/10.1016/j.ijggc.2017.05.011.
[58] Modelon AB, Modelon Home, 2018. <https://www.modelon.com/>.
[59] A. Johansson, F. Johnsson, B. Leckner, Solids back-mixing in CFB boilers, Chem. Eng. Sci. 62 (2007) 561–573, https://doi.org/10.1016/j.ces.2006.09.021.
[60] F. Johnsson, W. Zhang, B. Leckner, Characteristics of the formation of particle wall layers in CFB boilers, in: 2nd Int. Conf. Multiph. Flow, Kyoto, Japan, vol. 3, Kyoto, Japan, 1995.
[61] J. Eborn, On model libraries for thermo-hydraulic applications, Dep. Autom. Control. Lund Inst. Technol. (2001) 135. http://www.control.lth.se/documents/2001/ebo01phd.pdf.
[62] Springer, ed., VDI Wärmeatlas, 9th ed., Springer, 1997. <https://www.springer.com/gp/book/9783540778769>.
[63] K.S. Bhambare, S.K. Mitra, U.N. Gaitonde, Modeling of a coal-fired natural circulation boiler, J. Energy Resour. Technol. Trans. ASME. 129 (2007) 159–167, https://doi.org/10.1115/1.2719209.
[64] F. Casella, A. Leva, Modelica open library for power plant simulation: design and experimental validation, in: Proc. 3rd Int. Model. Conf., 2003, pp. 41–50. <http://scholar.google.com/scholar?hl=en&btnG=Search&q=intitle:Modelica+open+library+for+power+plant+simulation+:+design+and+experimental+validation#0>.
[65] K.J. Åström, R.D. Bell, Drum-boiler dynamics, Automatica 36 (3) (2000) 363–378.
[66] R. Paranjape, Modeling and control of a supercritical coal fired boiler, Texas Tech. Univ. (1996), https://doi.org/10.1080/00431672.1996.9925425.
[67] R. Beebe, Condition monitoring of steam turbines by performance analysis, J. Qual. Maint. Eng. 9 (2003) 102–112, https://doi.org/10.1108/13552510310482361.
[68] M.B. Dzodzo, B. Liu, A. Cioncolini, S.R. Spiegelman, Appl. CFD Model. Flows Feed-Water Pipel. (2006) 293–301, https://doi.org/10.1115/ICONE14-89549.
[69] S. Skogestad, Probably the best simple PID tuning rules in the world. AIChE Annu. Meet. Reno, NV, 2001.
[70] K.E. Haeggblom, Partial relative gain: a new tool for control structure selection, Aiche Annu. Meet. (1997).
[71] G. Martinez Castilla, M. Biermann, R.M. Montañés, F. Normann, F. Johnsson, Integrating carbon capture into an industrial combined-heat-and-power plant: performance with hourly and seasonal load changes, Int. J. Greenh. Gas Control. 82 (2019) 192–203, https://doi.org/10.1016/j.ijggc.2019.01.015.
[72] P.J. Dechamps, Modelling the transient behaviour of heat recovery steam generators, Proc. Inst. Mech. Eng. Part A J. Power Energy. (1995) 265–273, in: https://doi.org/10.1243/PIME_PROC_1995_209_005_01.
[73] H. Liu, T. Hibiki, Flow regime transition criteria for upward two-phase flow in vertical rod bundles, Int. J. Heat Mass Transf. 108 (2017) 423–433, https://doi.org/10.1016/j.ijheatmasstransfer.2016.12.029.
[74] H.C. Cooke, On prediction of off-design multistage turbine pressures by Stodolás Ellipse, J. Eng. Gas Turbines Power. 107 (July, 1985,) 596–606.
[75] O. Bolland, Therm. Power Gener. (2014).